Energy 305 (2024) 132290

Contents lists available at ScienceDirect

Energy

journal homepage: www.elsevier.com/locate/energy

Optically functional bio-based phase change material nanocapsules for highly efficient conversion of sunlight to heat and thermal storage

Oguzhan Kazaz [a], Nader Karimi [a,b], Manosh C. Paul [a,*]

[a] Systems, Power & Energy Research Division, James Watt School of Engineering, University of Glasgow, Glasgow, G12 8QQ, UK
[b] School of Engineering and Materials Science, Queen Mary University of London, London, E1 4NS, UK

ARTICLE INFO

Handling editor: Wojciech Stanek

Keywords:
Photothermal conversion and storage
Optically functional nanostructures
Bio-based phase change materials
Nanoencapsulation
Light-matter interaction

ABSTRACT

Conversion of sunlight to heat and the subsequent thermal storage by nanoencapsulated bio-based phase change material slurries (NBPCMSs) in a low temperature solar system is investigated. The influences of capsule size, shell material, tilt angle, solar heat flux, PCM mass concentration, nanoparticle and its concentration are explored. The results reveal that the useful heat gain capacity of nano-enhanced coconut oil/Ag, coconut oil/Au, coconut oil/Al, and coconut oil/Cu based slurries is respectively 3.02, 3.12, 2.7, and 3.14 times better than that of pure water, due to an enhanced interaction of light with the functional bio-based PCM nanocapsules. Consequently, the thermal energy storage is reported to be 8.85, 9.29, 7.41, and 9.19 times higher. The increment in mass concentration of PCM from 5 to 20 % and addition of blended nanoparticles further augment the solar thermal energy storage capacity. Specifically, the storage capacity of coconut oil/Au based slurry is improved by up to 74.4 % when the 20 % coconut oil is used as a core material. The energy storage improvements of Cu and Ag based slurries enhance by 4.04 and 4.87 %, respectively, with the insertion of Au nanoparticles at a volume fraction of 25 ppm. Augmenting the core/shell confinement size, on the other hand, diminishes the surface area to volume ratio, allowing agglomeration of the structures inside the slurry. The performance of solar energy storage decreases as the inclination angle of the storage cavity increases from 0° to 60°, reducing the buoyancy force and particles' collision. Further, since Al particles have low optical characteristics and thermal conductivity, the thermal performance of coconut oil/Al nanoencapsulated slurry are at the lowest level. Finally, experiment is conducted to validate the specific heat capacity model prediction under various wind speeds, from 1 to 4 m/s, and solar illuminations, from 400 to 1000 W/m^2.

Nomenclature

$K_{a\lambda}$	Absorption coefficient (1/m)	C_p	Specific heat (J/kgK)
P	Ratio of shell volume to total particle volume	ε_{bulk}	Metallic shell dielectric function
f	Shell concentration	C_{abs}	Absorption cross sections (cm^2)
T	Temperature (K)	C_p	Specific heat (J/kgK)
k	Thermal conductivity (W/mK)	L/H	Aspect ratio
A	Geometric parameter	$\vec{r}$	Position vector
$MPCS$	Microencapsulated phase change slurry	k	Absorption index
c_m	Mass concentration	h	Convective heat transfer coefficient
$\gamma(R)$	Scattering rate	Q_{abs}	Absorption efficiency of core/shell
N_T	Particle number in unit volume	r	Radius

(*continued on next column*)

(*continued*)

ε	Dielectric function	σ_s	Scattering coefficient (1/m)
w	Wind speed (m/s)	R	Effective mean free path
n	Refractive index	$\vec{s}'$	Scattering direction vector
V_f	Fermi velocity	C_{sca}	Scattering cross sections (cm^2)
I_λ	Radiation intensity (W/m^{2}μm)	τ_{bulk}	Bulk metal free electron scattering time
q	Heat (J/kg)	Greek symbols	
SA/V	Surface-area-to-volume ratio (1/m)	μ	Dynamic viscosity (Ns/m^2)
C_{ext}	Extinction cross sections (cm^2)	ϵ	Emissivity
p	Pressure (Pa)	ρ	Density (kg/m^3)
$\vec{s}$	Direction vector	Φ	Dissipation functions
$I_{b\lambda}$	Black body intensity (W/m^{2}μm)	Ω'	Phase function

(*continued on next page*)

* Corresponding author.
E-mail address: Manosh.Paul@glasgow.ac.uk (M.C. Paul).

https://doi.org/10.1016/j.energy.2024.132290
Received 15 May 2024; Received in revised form 27 June 2024; Accepted 1 July 2024
Available online 2 July 2024

(*continued*)

ΔH	Total enthalpy change (J/kg)	β	Thermal expansion coefficient (1/K)
$K_{e\lambda}$	Extinction coefficient (1/m)	λ	Wavelength of incident light (μm)
$\varepsilon_a, \varepsilon_b$	Effective dielectric function	σ	Stefan Boltzmann (5.67×10^{-8} W/m^{2}K^4)
E	Enhancement	Subscripts	
PCM	Phase change material	1	Core
α_λ	Spectral absorption coefficient (1/m)	s	Solidus
u, v	Velocity vectors (m/s)	amb	Ambient
α	Polarizability	2	Shell
w_p	Bulk plasma frequency	r	Radiative
H	Latent fusion heat (J/kg)	out	Outlet
Q_{sca}	Scattering efficiency of core/shell	3	Outer region
l_∞	Bulk free electron mean free path	l	Liquidus
ΔT	Temperature change (K)	bf	Base fluid
$NBPCMS$	Nanoencapsulated bio-based PCM slurry	in	Inlet
γ_∞	Inverse of the bulk relaxation time		

1. Introduction

Conventional fossil-origin fuels in energy generation provokes an escalation in carbon emissions, inducing the global warming impacts to be felt. Therefore, eminence of energy production from alternative sources such as solar energy has emerged [1]. However, the fact that sunlight is intermittent which restricts continuous solar energy usage. The solar energy's storage by converting it to thermal energy, therefore, ensures its use and efficiency. Nevertheless, due to the large difference between demand and supply in thermal energy applications, it often creates a low-level utilisation of solar energy [2]. To avoid this, thermal energy storage methods are used to help enhance the energy efficiency by storing excess heat and releasing it when needed. Sensible, latent, and thermochemical heat storage techniques are commonly used as thermal energy storage technologies [3]. However, a latent heat storage has more energy storage capacity than a sensible heat storage and it is also cost-effective compared to a thermochemical heat storage. Additionally. with its high thermal energy capacity in phase transformations of PCMs [4,5], thermal energy could be stored at a high rate and contributes to the use of this energy by releasing it when needed. Due to these advantages provided by PCM-based storage and thermal systems, its use in solar collectors has an upward trend [6,7].

Wang et al. [8] developed a new dual PCM based flat plate solar collector to prevent the overheating and freezing difficulties and experimentally investigated. Two different PCM layers were placed under the absorber wall with a melting temperature of 15 and 70 °C, and the influence of them on performance was compared. It was detected that the time needed to rise the temperature of the absorber wall from 60 to 78 °C increased by 1.6 h under an elevated temperature state. PCM with a low melting temperature was also uncovered to slow the collector's temperature drop by releasing heat and solidifying under the meagre temperature status. When the low melting point PCM sheet was settled above and below the high melting point PCM, the time for the temperature of the absorber wall to drop from 19 to 10 °C was extended by 6.4 and 3.1 h, respectively. The efficiency of the PCM-based collector was improved by 19.6 and 24.1 % compared toa conventional flat plate collector when the high melting point PCM sheet was settled above and below the low melting point of PCM, respectively. A novel PCM based hybrid photovoltaic solar energy collector (PVT-PCM) was developed by Li et al. [9]. They also analysed the system's energy saving potential and economic investigation. The experimental results revealed that the average power generation efficiency was 14 % higher than a conventional PV. The combined calculation of solar thermal usage efficiency and the solar combined utilisation rate were 24.2 and 39.4 %, respectively. They also recognized that the energy-saving and system efficiencies were 64.2 and 39.4 %, respectively. The PVT system's lifespan was estimated to be 25 years. It was further suggested that the additional payback of the system could be completed at the end of 13.1 years. In addition, it was reported that the highest CO_2 emission could be declined by 156,1 kg per year due to the local energy structure.

Nekoonam and Ghasempour [10] established a 2D effective heat capacity model to analyse the collector with integrated energy storage's thermal behaviour. The structure was composed of a synthetic oil as working fluid, encapsulated spherical capsules and PCM. Genetic Algorithm with using two scenarios was employed to solve the PCM's low thermal conductivity, enhance the system's efficiency and melting and for optimisation. The unit's outlet temperature with no temperature constraint was applied in scenario 1 while the unit's outlet temperature with threshold limitation was utilised in scenario 2. The outcomes indicated that a 5 % decrease of the inlet fluid temperature resulted in a 32 % enhancement (25 % reduction) in charging time and a 17 % decline (20 % increment) in total stored energy. It was also determined that 4725 and 4940 kWh of energy was stored by the ideal arrangement during charging in the 2nd and 1st scenarios, respectively.

In terms of material consideration for PCM, commonly used paraffin, which is a petroleum-origin material, could indirectly increase the fossil fuels utilisation and also pose the risk of hazardous and unsavoury factors to the habitat [11]. In addition, the fact that paraffin is a flammable material limits its operation [12]. Therefore, implication of a bio-based PCM which could be derived from natural sources such as plant or animal fat seems to be a promising alternative [13]. It is also recognized as an energy storage material for thermal systems including cooking or edible oils such as coconut oil [14] due to their no oxidation and thermally balanced characteristics [15]. Because of these advantages, the use of natural-based PCMs in solar systems is also becomes an important research direction [12,16]. For example, Prasannaaa et al. [17] considered fatty acid based PCM for thermal control of photovoltaic panel and compared the results without and with PCM. The mean efficiency was also enhanced by 9.43 % in March and by 10.31 % in December. Using stearic acid as PCM, a new solar collector was developed and experimentally analysed by Chopra et al. [18]. The collector's thermal capacity was investigated and compared using different flow rates. The PCM efficiency was varied from 61 to 64 % and the suggested system's annual fuel and cost were also reported to be better than a standard method. It was found that the cost of capital could be recovered after 6 years of process. On the other hand, Xu et al. [19] investigated a solar photovoltaic/thermal system combined with PCM (PV/T-PCM) using fatty acid with a melting point of 37 °C as PCM. Metal fins were also used to augment heat transfer. They carried out four-day experimental studies in outdoor climatic cases. The solar collectors of Case 1 and Case 2 were executed with dual-axis tracker while Case 3 and Case 4 were kept stationary case. Two dissimilar periodic thermal regulation procedures employing the water circulation in the system to enhance the sunlight utilisation efficiency were studied and compared. It was reported that the PCM enhanced the photoelectric efficiency by reducing the temperature oscillation. The maximum efficiency was obtained at a setting temperature of 45 °C as 91 % for Case 1 and Case 3 while the efficiency of Case 2 and Case 4 was 85 % at a regulation temperature of 50 °C. Although the fatty acid had low thermal conductivity, temperature stratification due to metal fins was important. It was noticed that lower temperature regulations resulted in the higher heat removal from the PCM.

Low thermal conductivity and leakage problems, on the contrary, can be seen as a limiting factor for storage performance apart from the PCMs' high thermal energy storage properties. By encapsulation, PCMs can be covered by a protective layer, to prevent their leakages as they are confined within the shell during phase transformations [2,20,21]. Hu et al. [1] experimentally scrutinised the photothermal conversion of spent coffee grounds (SCGs) based composite PCMs (CPCMs). Reduced graphene oxide (RGO) was employed as a shell substance to impede

leakage while also to improve the shape stabilisation. The RGO improved the SCG's adsorption and radiation absorption and thermal conductivity of CPCMs in Ultraviolet/Visible/Near Infrared range. No chemical connection between the SCGs@RGO and PEG was found and as the RGO's weight concentration enhanced, the PEG's crystallinity was improved. Furthermore, the PEG/SCGs@RGO's crystallization and melting temperature was not altered compared to pure PEG, but its enthalpy efficiency augmented by 98.6 %. The PEG/SCGs@RGO's crystallinity, chemical and thermal characteristics remained unchanged despite the 100 heating and cooling cycles. It was also regarded that the PEG/SCGs@RGO's release functions and energy storage did not modify in spite of 10 photothermal transformation periods. Microencapsulated lauric acid (LA) as a PCM with a polystyrene shell utilising an emulsion polymerization method was developed by Sami et al. [22]. The capsules' thermal durability, morphology and thermal characteristics were analysed using thermogravimetry analysis, Scanning Electron Microscopy, and differential scanning calorimeter. Sodium dodecyl sulfate (SDS) to styrene (St) mass ratio, lauric acid to styrene mass ratio, temperature and stirring rate on the microencapsulation ratio (ME. R) were considered and examined. The experimental outcomes indicated that the developed microencapsulated PCM had a latent heat of 167.26 kJ/kg and a transition temperature of 43.77 °C. However, the temperature and stirring speed had no impact on ME. R (%). In particular, the ME. R was improved compared to earlier works and achieved as a maximum of 92.3 %. The best values of temperature, LA/St mass ratio, ME. R, stirring speed and SDS/St mass ration were 55 °C, 0.42, 91.64 %, 1076 rpm, 0.01, respectively. Wang et al. [23] developed a novel PCM by enhancing the thermal conductivity and enthalpy change for energy conversion and storage applications. The shape stable phase change materials composites (ss-PCMCs) were composed of organic PCMs (palmitic acid (PA) and 1-hexadecanamine (HDA)) into the biomass carbon aerogels (BCAs). The sunflower stem carbon aerogel (s-CA) and sunflower receptacle spongy carbon aerogel (r-CA) constituted the BCAs. According to experimental results, the new composite PCMs had superior phase transformation enthalpy that ranged from 207.9 to 271 kJ/kg. It was further observed that the enthalpy remained almost constant despite 50 times of freezing/melting periods. The BCAs-based composite PCMs' thermal conductivity improvements were 1.85 and 2.54 times better than that of PA and HAD based PCMS, respectively. Impotantly, the photothermal conversion performances of HDA/s-CA and HDA/r-CA were 67.8 and 75.6 %, respectively.

The volumetric radiation's impacts come to the fore in storage systems that are immediately heated by the sun's rays of the energy storage material. Phase change slurries made by dispersion of composite PCMs in the solution like water, therefore, can be utilised in solar collectors to further enhance the radiation's power in the fluid medium [24–26]. The thermal capacity of a direct absorption evacuated tube collector employing a mixing of microencapsulated phase change material (MPCM) and nanofluids was numerically evaluated by Karami et al. [27]. Flow velocity, volume concentration and different host fluids (ethylene glycol (EG) and water) were examined by varying operating conditions. The outcomes showed that water and EG based blended nanofluids of CuO/Al_2O_3 particles were better in terms of performance of heat storage than CuO nanoparticle based nanofluids. In addition, as the volume concentration enhanced, the system efficiency improved by augmenting the attenuation of nanofluids. The collector's capacity was also augmented by diminishing the heat loss to the atmosphere as the fluid flow rate enhanced. It was further indicated that a mixture of MPCM and CuO nanofluid enhanced the efficiency by 4.53 % with reducing the heat loss by 5.84 %. The maximum efficiency was achieved by employing the mixture of CuO nanofluid and MPCM as 76.28 %. Bohdal et al. [28] studied a microencapsulated PCM slurry based flat plate solar collector. The influences of mass concentration (0, 4.3, and 8.6 %), irradiation density (270–880 W/m^2), and volume flow rates (30, 40, 60, and 80 kg/h) were examined. Their experimental results also reported that the system performance was enhanced by PCM capsules compared to water due to the enhancement of fluid's temperature. Their findings also expressed that the slurry-based collector enhanced the fluid's temperature increment more by reducing the heat losses to the surroundings. Yuan et al. [29] developed novel microencapsulated PCMs where paraffin and silica and graphene oxide (GO)-grafted SiO_2 were utilised as core and shell materials, respectively to experimentally scrutinise the solar-to-thermal energy conversion performance. The transformation temperature of the paraffin@SiO_2 and paraffin@SiO_2/GO were almost the same as paraffin. The encapsulation ratio was 50.8 and 49.6 % in the paraffin@SiO2 and paraffin@SiO2/GO composites, respectively. The paraffin@SiO_2/GO had the better thermal balance and reliability. They also prepared slurries by dispersing the paraffin@SiO_2 and paraffin@SiO_2/GO microcapsules in water, and it was found that their specific heat capacities were higher than water. The results also unveiled that the paraffin@SiO_2/GO based slurry's thermal capacity was better than that of paraffin@SiO_2 based slurry due to the higher thermal conductivity and heat capacity.

1.1. Contribution of this paper

Although it has been explained in the literature that PCMs and phase change slurries are deployed to augment the overall performance in solar energy applications, no study has been found on the bio-based PCM slurries' effect on the solar system with a participating medium. The study presented in this paper will concentrate the applications of NBPCMS in a solar system under the influence of direct radiation as volumetric heating. The innovations of this work can, hence, be summarised as follows.

- A storage system where the sun's rays are instantly absorbed by the energy storage material may have a slope angle as it must be installed either on a roof or on ground. Since the alteration in the inclination angle may compel variations in the fluid's buoyancy effects, it can alter the free convection and particles' collision with each other. How do these combined affect the heat generation inside a solar collector?
- Modification in the nanoencapsulated PCMs' structural properties, called nano-enhanced PCMs, may also amend the fluid's capability to absorb sunbeam. Since these adjustments in the shell type and thickness, as well as the transformation in the core size, manipulate the optical properties due to the surface plasmon, the nanocapsules' thermal performance under the impact of interaction of light with matter will be examined and how these variations reshape the behaviour between the solar radiation and nano-enhanced PCMs.
- Besides, a new type of hybrid slurries based on the optically functional coconut oil nanocapsules formed with mono- and blended-nanoparticles dispersed in the base fluid will be studied to improve the energy storage by altering the slurry's optical properties as a result of the light-matter interaction in the translucent medium, where the absorption-scattering-emitting effects are effective. How will these radiative properties change the system's thermal capacity by employing these new heat transfer fluids?

Consequently, the first analysis of the combined effects of free convection-inclination angle and radiation-particle interaction in a NBPCMS is done by using coconut oil as PCM due to its melting and phase transition. When these are assessed, the endeavour of the present research is to develop an innovative slurry to fulfil the abovementioned research gaps related to the solar energy conversion and storage capabilities by computational parametric investigation. Finally, the thermal performance of the cavity filled with solid coconut oil as PCM is experimentally investigated at different radiation heat fluxes and wind speeds. The melting fractions are also compared for the effective heat capacity model's validation, which is another new contribution as there is insufficient experimental study on this topic.

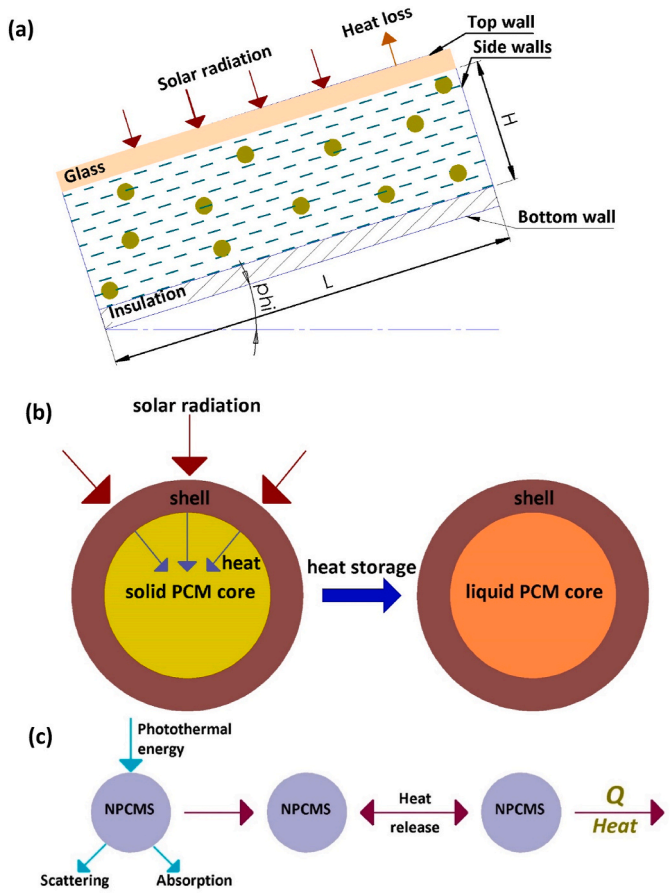

Fig. 1. The schematic of the NBPCMS based solar system, (b) optically functional bio-based PCM nanocapsules, and (c) impact of photothermal energy on a bio-based nano capsule inside the slurry.

2. Modelling and methodology

A 2D model of NBPCMS based solar collector having an aspect ratio, *L/H,* of 10 [30] is presented in Fig. 1(a). The collector's upper wall is surrounded by a glass coating so that the sun's rays can be absorbed by the slurry. The other walls, however, are regarded as adiabatic to enhance the system's storage capacity. The convection coupled with radiation heat loss takes place from the top wall to the environment.

The core and shell structures, as in Fig. 1(b), form the nano-encapsulated PCM as a composite material. The temperature of the solid PCM, which makes up the core, boosts with the advance of solar energy and achieves the phase change temperature. Thus, the solid PCM begins to melt, turning to liquid. The PCM surrounded by the protective shell material hinders leaks throughout the phase transformations, impeding blending with the base fluid. The composite PCMs made of metal-based shell materials capture sunlight as in Fig. 1(c). Moreover, these composite materials, which are uniformly dispersed in water, start to collide with each other to catch these rays.

The equation of Radiation Transport to compute the radiation's spectral attenuation is determined as [31]:

$$\nabla \bullet (I_\lambda(\vec{r},\vec{s})\vec{s}) + (\alpha_\lambda+\sigma_s)I_\lambda(\vec{r},\vec{s}) = \alpha_\lambda n^2 I_{b\lambda} + \frac{\sigma_s}{4\pi}\int_0^{4\pi} I_\lambda(\vec{r},\vec{s}')\Phi(\vec{s}\bullet\vec{s}')d\Omega' \quad (1)$$

The scattering/absorption efficiencies and extinction coefficient of the composite structure are determined as [32–34]:

$$Q_{sca} = C_{sca} / (\pi a^2) = \frac{128\pi^5}{3\lambda^4}\varepsilon_3^2 r_2^6 \left|\frac{\varepsilon_2\varepsilon_\alpha - \varepsilon_3\varepsilon_b}{\varepsilon_2\varepsilon_\alpha + 2\varepsilon_3\varepsilon_b}\right|^2 \Big/ (\pi a^2) \quad (2)$$

Table 1
Thermophysical properties of the materials [46–50].

	H (J/kg)	C_p (J/kgK)	k (W/mK)	ρ(kg/m^3)
Solid coconut oil	103250	3750	0.228	920
Liquid coconut oil		2010	0.166	914
Cu		383	400	8954
Ag		235	429	10500
Al		900	247	2700
Au		128.8	314.4	19320

$$Q_{abs} = C_{abs} / (\pi a^2) = \frac{8\pi^2\sqrt{\epsilon_3}}{\lambda} r_2^3 Im\left(\frac{\varepsilon_2\varepsilon_\alpha - \varepsilon_3\varepsilon_b}{\varepsilon_2\varepsilon_\alpha + 2\varepsilon_3\varepsilon_b}\right) \Big/ (\pi a^2) \quad (3)$$

$$K_{e\lambda} = (\pi a^2(Q_{abs}+Q_{sca}))(6f/\pi D^3) \quad (4)$$

The total attenuation coefficients of composite PCM and water $(K_{f,e\lambda} = 4\pi k/\lambda)$ is equal to the extinction coefficient of the slurry as:

$$K_{total,e\lambda} = K_{f,e\lambda} + K_{e\lambda} \quad (5)$$

The Drude model is also utilised to compute the dielectric function of the composite structure as the construction changes due to the shell materials [35,36].

$$\varepsilon(w) = \varepsilon_{bulk}(w) + \frac{w_p^2}{w^2 + iw\gamma_\infty} - \frac{w_p^2}{w^2 + iw\gamma(R)} \quad (6)$$

In addition, a detailed explanation of the above equations with their constants for the optical modelling is given in the previous work of the authors [37,38]. The water and composite PCM's optical constants are also obtained from the literature [39–42].

The NBPCMS is presumed to be incompressible, Newtonian, laminar, and single-phase. The conservation equations in a tilted solar system are defined as:

$$\frac{\partial u}{\partial x} + \frac{\partial v}{\partial y} = 0 \quad (7)$$

$$\rho_{slurry}\left(u\frac{\partial u}{\partial x} + v\frac{\partial u}{\partial y}\right) = -\frac{\partial p}{\partial x} + \mu_{slurry}\left(\frac{\partial^2 u}{\partial x^2} + \frac{\partial^2 u}{\partial y^2}\right) + g\sin\phi(\rho\beta)_{slurry}(T - T_o) \quad (8)$$

$$\rho_{slurry}\left(u\frac{\partial v}{\partial x} + v\frac{\partial v}{\partial y}\right) = -\frac{\partial p}{\partial x} + \mu_{slurry}\left(\frac{\partial^2 v}{\partial x^2} + \frac{\partial^2 v}{\partial y^2}\right) + g\cos\phi(\rho\beta)_{slurry}(T - T_o) \quad (9)$$

$$\rho_{slurry}C_{p_{slurry}}\left(u\frac{\partial T}{\partial x} + v\frac{\partial T}{\partial y}\right) = k_{slurry}\left(\frac{\partial^2 T}{\partial x^2} + \frac{\partial^2 T}{\partial y^2}\right) - \nabla \bullet q_r \quad (10)$$

The system's boundary conditions, consequently, are displayed as: at the side walls:

$$\frac{\partial T}{\partial x} = 0 \quad (11)$$

at the top wall:

$$q = h(T - T_{amb}) + \varepsilon\sigma(T^4 - T_{amb}^4) \quad (12)$$

at the base wall:

$$\frac{\partial T}{\partial y} = 0 \quad (13)$$

at the wall surfaces:

$$u = v = 0 \quad (14)$$

where h is determined as [43]:

$$h = 5.7 + 3.8v \quad (15)$$

Fig. 2. 2-D non-uniform mesh generation.

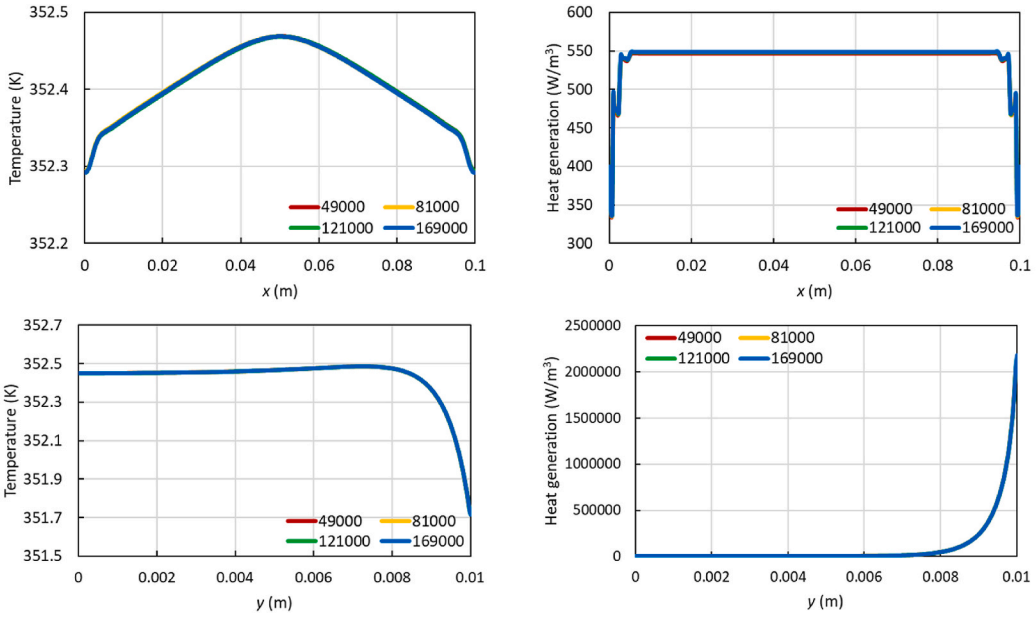

Fig. 3. Impact of different mesh sizes along horizontal and vertical midlines at tilt angle of zero degree for coconut oil/Au nanoencapsulated PCM slurry.

Table 1 displays the thermophysical properties of the shell materials and PCM. The conservation equations depend on the choice of NBPCMS and further information can be found in Refs. [37,38]. This study also compares the performance of a pure nanofluid and slurry and the modelling of nanofluids was already detailed in the earlier studies of the authors [44,45].

The heat gain and stored energy in the solar system are respectively defined as [51,52]:

$$q_{heat\ gain} = C_p\ \Delta T \tag{16}$$

$$q_{stored\ energy} = \Delta H \tag{17}$$

where the slurry's specific heat, C_p, involves the phase change, and it is based on the temperature of melting and solidifying. The former research [37,38] of the authors also extensively explained the slurry's specific heat capacity model. The slurry, which has an initial temperature $T_{initial}$, is heated by the influence of solar energy and reaches the final uniform temperature, T_{final}. Thus, the temperature gain/change, ΔT, of the slurry is equal to $T_{final} - T_{initial}$. The slurry's enthalpy change, ΔH, also depends on the temperature difference.

Lastly, the thermal augmentation between the cases of the host fluid and slurry can be explained as:

$$E = \frac{(computational\ value)_{slurry} - (computational\ value)_{host\ fluid}}{(computational\ value)_{host\ fluid}} \tag{18}$$

where the computational value demonstrates either the stored thermal energy or temperature/heat gain.

2.1. Numerical procedure and grid dependency test

A pressure-based finite volume method is employed to solve the energy transport and Navier-Stokes equations with ANSYS Fluent 2020-R1. By choosing the Discrete Ordinates (DO) radiation method, the Radiation Transport equation including the absorption, emission and scattering impacts is solved. The energy and DO radiation equations' residual levels are remained below 10^{-6}, whilst the other equations are also kept below 10^{-5} to get more consistent findings. Moreover, a comprehensive information for the numerical procedures can be found in the authors' previous works [37,44,45].

A grid dependence test is performed by selecting various grid sizes of 49000, 81000, 121000 and 169000, keeping a high mesh resolution close to the walls, as shown in Fig. 2. Their effects in the volumetric absorbed radiation and temperature for pure water and coconut oil/Au nanoencapsulated PCM slurry are negligibly small as indicated in Fig. 3. In addition, the impacts of these mesh numbers on the different tilt angles are also examined in Table 2. Based on the findings, 81000 grid sizes are chosen for further investigations, which ensure numerically stable results at a compromised cost for computation.

Table 2
Impact of various grid sizes with varying inclination angles.

Tilt angle (∘)	Mesh size	Average working fluid temperature (K)	Enthalpy change (kJ/kg)	Average volumetric absorbed radiation (kW/m^3)
0	49000	352.3613	461.24	92.760
	81000	352.361	461.238	92.760
	121000	352.3607	461.235	92.759
	169000	352.3605	461.233	92.759
30	49000	345.7986	405.403	80.209
	81000	345.7942	405.366	80.201
	121000	345.7913	405.342	80.195
	169000	345.7892	405.324	80.191
60	49000	328.1898	255.585	46.309
	81000	328.1873	255.563	46.304
	121000	328.1857	255.549	46.301
	169000	328.1845	255.539	46.298

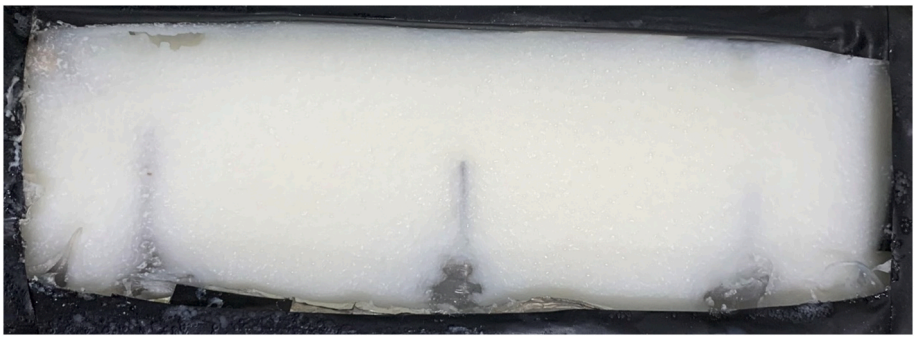

Fig. 4. Solid coconut oil.

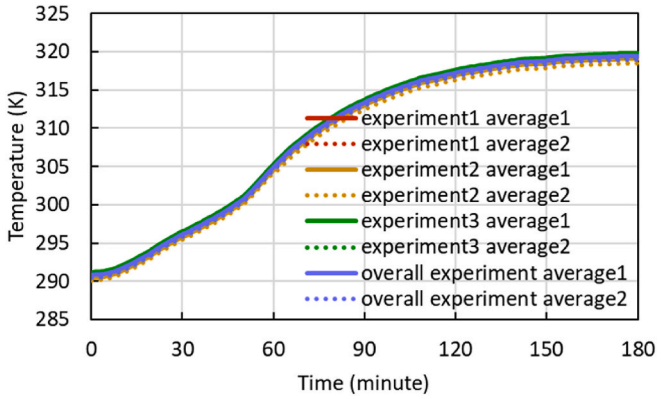

Fig. 5. Experimental system's stability investigation.

3. Experimental procedure

The lab scale test ring is set up for the validation of the specific heat capacity model for phase change process using pure solid coconut oil as a bio-based PCM as demonstrated in Fig. 4. It is subject to the coconut oil's temperature variation, and is determined as [53]:

$$C_p = \begin{cases} C_{p,s} & T < T_s \\ \dfrac{C_{p,s} + C_{p,l}}{2} + \dfrac{H}{T_l - T_s} & T_s < T < T_l \\ C_{p,l} & T > T_l \end{cases} \tag{19}$$

The experimental test system used in this study is designed by the authors and the picture of experimental setup, schematic format of experimental system and experimental procedure are explained in-detail in the authors' previous research to investigate the phase change process of RT28HC which is a kind of carbon-based PCM [38].

4. Results and discussion

This section has three sub-parts, starting with experimental outcomes, numerical validation accompanied by the computational results' investigation.

4.1. Experimental results

Fig. 5 clarifies the PCM average temperature profiles for three repetitions of a charge state. Two different average temperature values are used. Three thermocouples in the cavity are used for the first mean temperature, while six thermocouples are employed for the second mean value. As indicated in Fig. 5, a good repeatability is observed in the experiments performed under the same conditions. In addition, the reason why two different average temperature are almost the same is

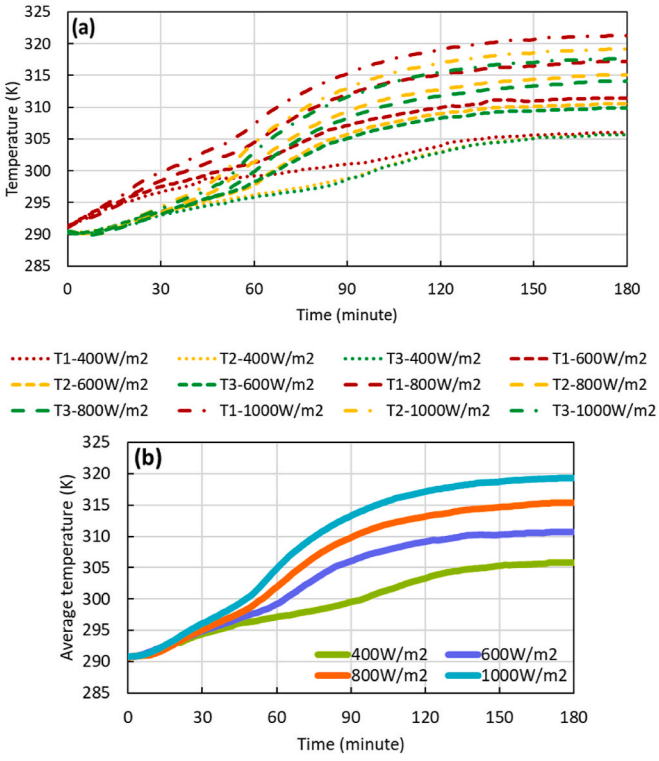

Fig. 6. Coconut oil's melting features inside the cavity under diverse solar fluxes (a) temperature curves with different cavity heights and (b) mean temperature curves.

that the temperatures of the thermocouples located at the same level horizontally are very close to each other. This is revealed the necessity of positioning the thermocouples in the cavity at different heights. It is also observed that the liquid coconut oil reached a stable state after the 150th minute. Finally, the time-dependent performance of the results and their stability analysed as done in Ref. [54]. For that, the experiment is conducted by applying the same three experiments keeping the same working, initial, and boundary conditions. As seen in Fig. 5, the standard deviation of the results is below 1.

Fig. 6 describes the PCM's charging process under different thermal radiations. As a result of moving the sun simulator vertically, dissimilar heat fluxes are obtained. Fig. 6(a), firstly, exhibits the thermocouples' behaviour at diverse layers in storage cavity against the different heat fluxes. T_1, T_2, and T_3 represent the temperature measurements from the cavity's upper, middle, and lower parts, respectively. Accordingly, it is noticed that the highest temperature inside the cavity is obtained in the upper region. It is also revealed that the temperature increment diminishes as one goes towards the cavity's base. This temperature gain or

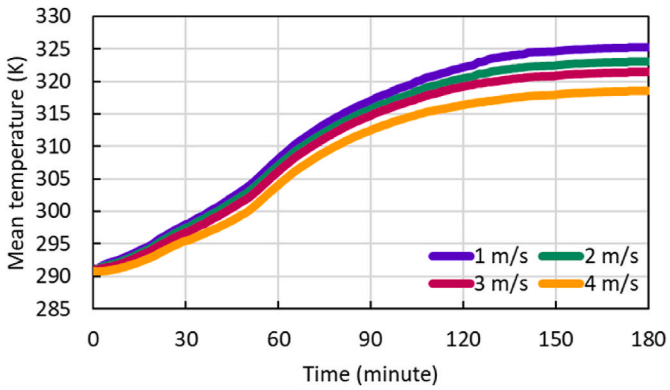

Fig. 7. Experimental average temperature of coconut oil under different wind velocities.

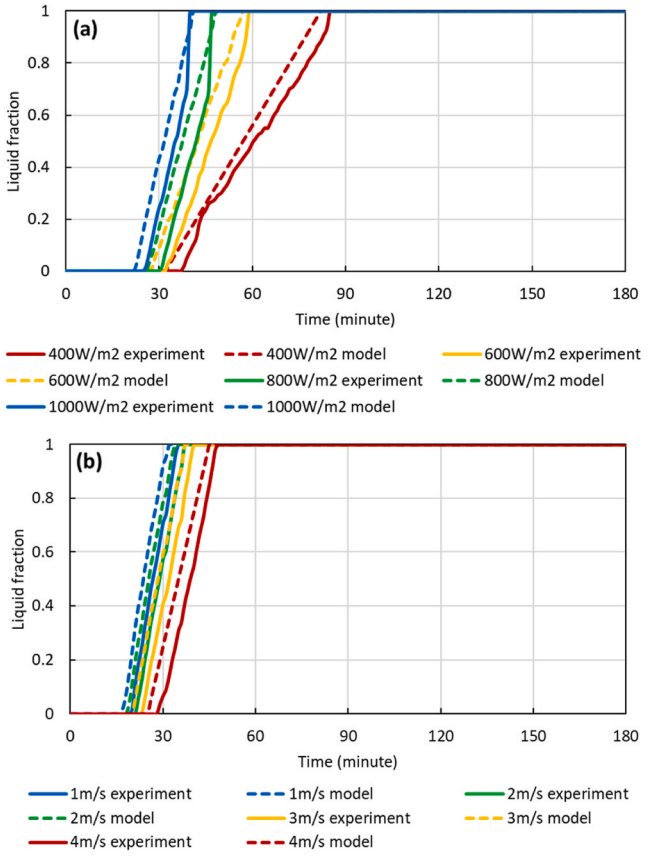

Fig. 8. Impact of various (a) heat fluxes and (b) wind speeds on coconut oil's liquid fraction behaviour.

temperature difference, however, declines as the solar flux decreases from 1000 to 400 W/m^2. The possible reason for this may be the decrease in the capacity of the coconut oil, which starts to melt due to the decreasing radiation, to capture this heat source. It, thus, causes the thermocouples' temperature gains in the cavity to be almost the same. In addition, the inducement why the temperature gain of T_1 is extreme at the beginning when the solar heat flux is 400 and 600 W/m^2 is that the solid PCM starts to melt from the top, increasing the effect of radiation on liquid molecules.

Fig. 6(b) also emphasizes the PCM's mean temperature performance. Increasing the solar flux from 400 to 1000 W/m^2 means that a stronger heat source penetrates the energy storage material. This provides an increase in the average temperature increment by improving the heat flow. Further, weakening the heat source impact causes the solid PCM to begin to melt later. In other words, it means an increase in the duration of the storage material in the liquid + solid phase. This time, which increases with weak radiation, prevents further heat gain of the PCM, which has become completely molten. Finally, the studied PCM average temperature behaviour, that enhances as a function of time, is consistent with the investigation of Siyabi et al. [55] and Sodhi et al. [56] who investigated the melting behaviour of PCM.

As illustrated in Fig. 7, the wind speed variation, which is another aspect altering the material's thermal capacity, on the average temperature increment is different. As the wind speed decreases or enhances, the heat dissipation from the storage cavity's glass panel to atmosphere alters. An enhancement in the speed from 1 to 4 m/s means that more intense convection currents fluctuate the collector. These increasing currents augments the heat losses to the surrounding and diminish the PCM temperature increment, thus reducing the liquid coconut oil's heat capacity. This finding is also consistent with the examination of Liu et al. [57] and Khanna et al. [58].

4.2. Validation

The specific heat capacity model is validated using liquid/melt fraction of the solid coconut oil. The liquid fraction represents the ratio of the total volume of a PCM occupied by liquid. It is affected by the solidification, melting and instant temperature of the PCM. Therefore, it can be defined as [59]:

$$\gamma = \begin{cases} 0 & T < T_s \\ \dfrac{T - T_s}{T_l - T_s} & T_s < T < T_l \\ 1 & T > T_l \end{cases} \tag{20}$$

Fig. 8 compares the melt fractions of coconut oil experimentally and numerically. It is seen that a good validation is obtained. In Fig. 8(a), it is displayed that the solid PCM begins to melt earlier with the improvement of the heat flux. This is because the heat source influences the PCM more intensely. The PCM's temperature increment, which starts to melt early, augments with the improved heat flux as in Fig. 6(b). In addition, the diminish in the wind speed means less heat losses. As indicated in Fig. 8(b), the temperature gain of PCM, which melts later with enhancing the wind speed, decreases compared to the others as in Fig. 7. Moreover, the liquid fraction performance as a function of period is coherent with that of Tao et al. [60] and Sodhi and Muthukumar [56]. Lastly, the augmented wind speed/heat flux and time-dependent alterations of melt fraction is assisted by the work of Liu et al. [57].

The mean absolute error (*MAE*) can be calculated to evaluate the reliability of the numerical model as a statistical analysis and is computed as [61]:

$$MAE = \frac{1}{N_{data}} \sum_{n=1}^{N_{data}} \left(T_{num,n} - T_{exp,n} \right) \tag{21}$$

where T_{exp} and T_{num} are the experimental and numerical temperature results respectively, and N_{data} is the total quantity of temperature recorded during the experiment. The numerical results as illustrated in Fig. 8 agree well with the experimental analysis as *MAE* is only less than 0.65.

The experimental scrutiny enacted by Goel et al. [62] is chosen to verify specific heat capacity method based on MPCS with the flat tube of length 0.3 m and diameter 3.14 mm. Water and N-eicosane are adopted for base fluid and PCM, respectively. The rate of the suspension's sensible heat capacity to its latent heat represents the Stefan number. The current wall temperature results coordinate with the benchmark model (Fig. 9(a)). The water based SiO_2/Au core/shell configuration is chosen for the radiation model which is conducted by Lee et al. [63]. The radiation penetrates the collector's upper panel with 1367 W/m^2 and has heat dissipation to the surrounding as 10 W/m^{2}K. The ambient

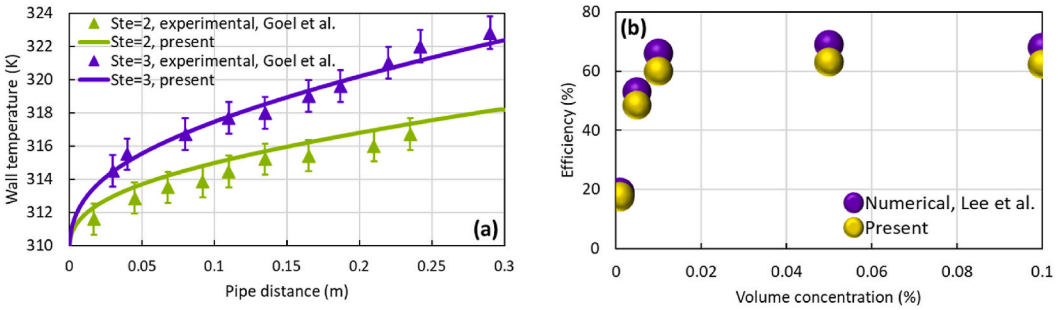

Fig. 9. Comparative analysis of the numerical model with published studies: (a) temperature through flow direction [62], and (b) collector efficiency as a function of nanoparticle concentration [63].

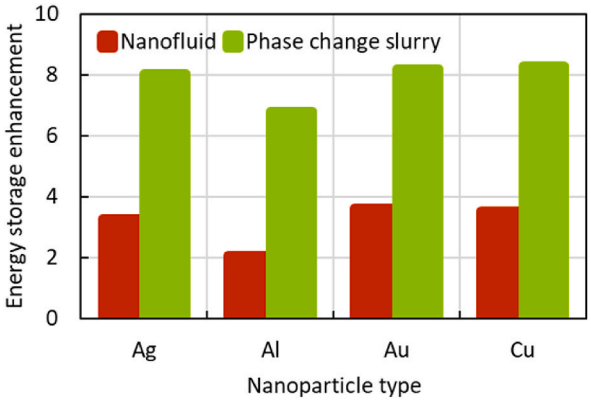

Fig. 10. Thermal capacity interpretation of nanofluid and nano-enhanced bio-based PCM slurry.

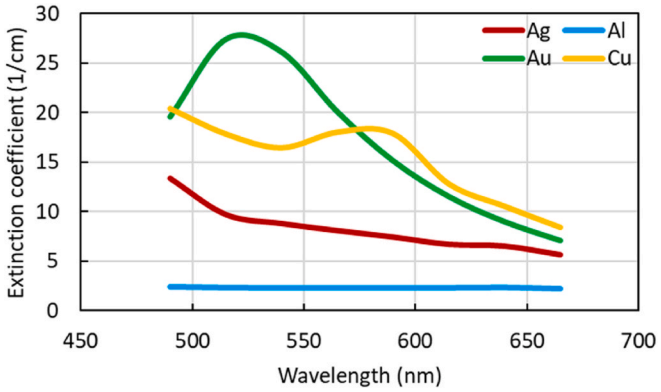

Fig. 11. Impact of different shell materials on nanoencapsulated bio-based PCM's optical properties as a function of wavelength.

temperature as 293.15 K is equal to fluid inlet temperature. The computational results coexist well with literature as an average error of 8.5 % (Fig. 9(b)).

4.3. *Numerical analysis of solar-to-thermal energy conversion and storage capacity*

The validation studies confirm that the present numerical scheme can be extended to further in-depth examination of the influence of coconut oil based nanoencapsulated phase change slurry on solar-to-thermal energy conversion and storage performance. PCM mass concentration, shell type, particle dimension, nanoparticle impact and heat flux, therefore, are considered as the main factors that can alters the system capacity. The nanocapsules' size is also akin to another research such as [37,64–67].

4.3.1. *Comparative analysis of phase change slurry and nanofluid*

The solar thermal energy storage capacity is analysed using slurry and nanofluid and compared. Ag, Al, Au, and Cu nanofluids are obtained by dispersing different types of metallic nanoparticles into the water. These metallic materials are used as shell material by surrounding the PCM in order to prevent the mixing of coconut oil selected as PCM with the base fluid throughout the form transformation from solid to liquid state and to improve its thermophysical properties. Nano-advanced bio-based PCM capsules, thus, are acquired. Au, Cu, Ag, and Al based slurries are formed by dispersing these nanocapsules into the system in which water is selected as the host fluid. As clarified in Fig. 10, the stored thermal energy augmentations of Au, Cu, Ag, and Al water-based nanofluids are 3.5, 3.6, 3.2, and 2.1 respectively. The storage enhancement in the thermal energy, however, improves by 137, 128, 224, 153 % respectively, with the augmentation of Au, Cu, Al, and Ag-shelled coconut oil-based composite confinements to water. This improvement, which takes place visibly, is the coconut oil's high latent heat capacity. This ability enhances the system's storage capacity by absorbing this latent heat when it approaches the phase transformation temperature of solid coconut oil. Hence, it is clearly seen that the PCM-based slurries considerably augment the solar energy conversion and storage compared to nanofluids.

4.3.2. *Effect of inclination angle coupled with shell character on thermal performance*

The impact of different shell materials coupled with varying PCM mass concentration is analysed in the tilted solar energy storage system in this part. While the coconut oil is employed as PCM, the nano-encapsulated PCMs are prepared by choosing silver (Ag), aluminum (Al), copper (Cu), and gold (Au) particles as shell materials, and slurry is obtained by dispersing them uniformly in pure water. In addition, 5, 10, 15 and 20 % are determined as PCM mass concentrations to prevent the fluid's non-Newtonian behaviour [68].

The combined effect of PCM and shell materials on optical performance is, firstly, shown in Fig. 11. The results indicate that the attenuation/extinction coefficients of the nanocapsules shift towards the long wave region (red). Ag, Al, Cu and Au particles activate free electrons in their shell structures due to their metallic properties under the influence of sunlight. This is a denouement of the surface plasmon resonance impact, that incites different peak positions to occur. The shifting and peak formation of the core/shell confinement are also consistent with those reported in Wu et al. [34]. Even though the Ag and Al shelled coconut oil tendencies in the extinction coefficient appear to be the identical (the absence of a peak), it is observed that the peaks are more prominent in Au and Cu shell materials. This is likely due to their stronger optical properties. It is also noticed that Al particles have the lowest attenuation coefficient due to their low optical properties.

After examining the nanocapsules' optical properties, it is necessary

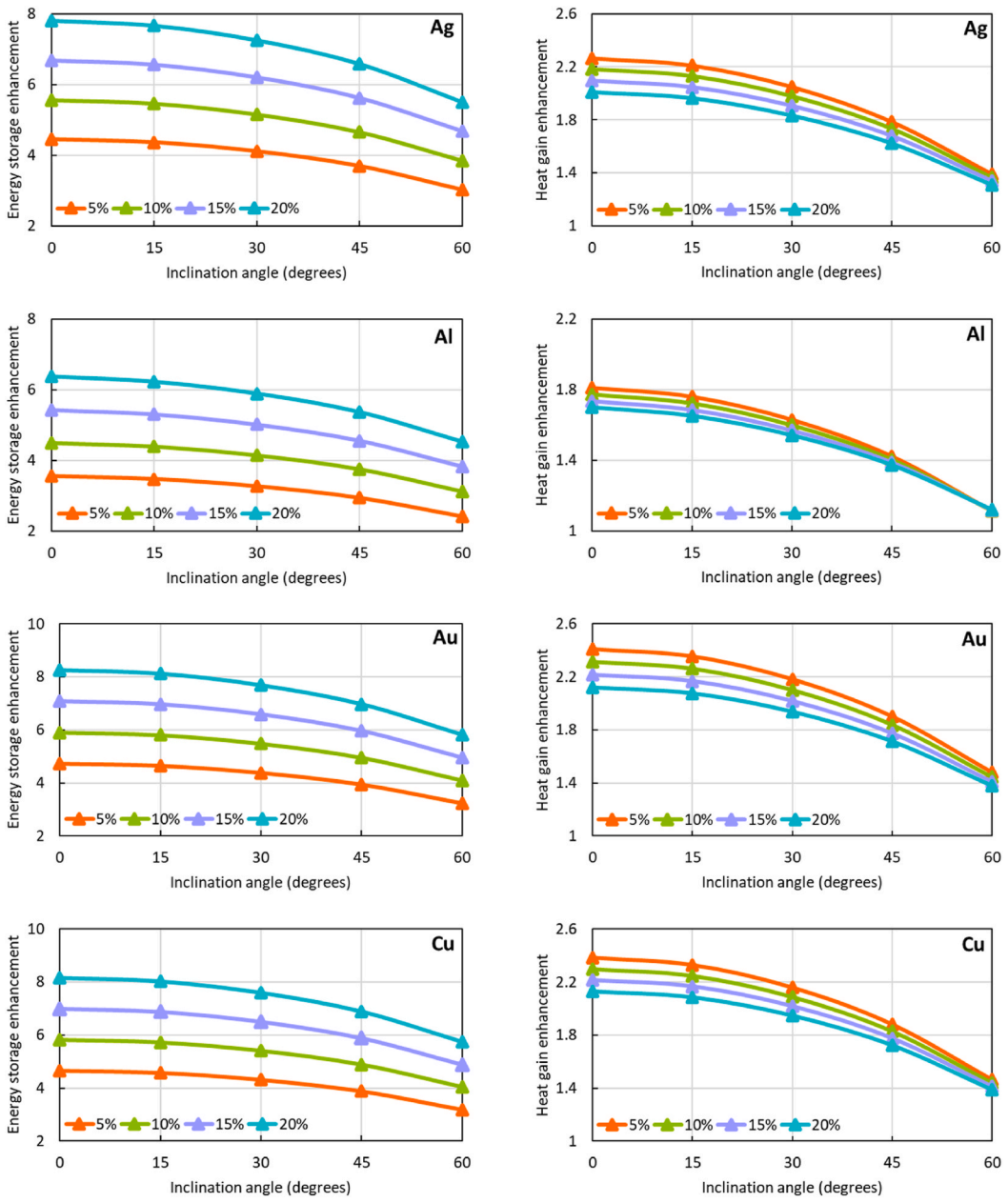

Fig. 12. Effects of PCM mass fraction, shell matter, and inclination angle on solar thermal storage (left pillar) and heat gain (right pillar) augmentations.

to investigate the slurry's thermal performance. The slurry's thermo-physical properties and the tilt angle of the storage system affect the thermal capacity as well as the optical behaviour.

Al shelled nanocapsules have the lowest attenuation coefficient as indicated in Fig. 11. It is also not surprising that the coconut oil/Al slurry has the poor thermal performance as a result of these two combined effects, with Al particles having a lower thermal conductivity coefficient (Fig. 12). The energy storage enhancement is 4.45, 3.56, 4.73, and 4.66 of nano-enhanced coconut oil/Ag, coconut oil/Au, coconut oil/Al, and coconut oil/Cu based slurries, respectively when the inclination angle and PCM mass concentration are 0° and 0.05, respectively. In addition to the insufficient absorption of solar rays by the Al shelled nanocapsules, the inadequate heat exchange between the base fluid and the nano-capsules causes the solar energy to thermal energy conversion to occur at a minimum. Furthermore, the coconut oil/Au and coconut oil/Cu slurries are realized to have alike and better performance (Fig. 12). The average extinction coefficient of Cu and Au shelled nanocapsules is quite same. Although the Ag particles' thermal conductivity is higher, the average extinction coefficient is lower than the Cu and Au shelled nanocapsules. This provokes less sunbeam to be absorbed by the slurry. The coconut oil/Ag slurry's capacity, thus, remains low.

The PCM mass concentration alters the enthalpy and temperature increments of the slurry. In terms of fixed slope, it is recognized that as the mass fraction improves to 20 %, it diminishes the heat gain and improves the thermal storage (Fig. 12). While the coconut oil transforms from solid to liquid state, there is not much alteration in the temperature change during phase transformation due to its latent thermal capacity. Therefore, when the core in the core/shell structure is filled with higher PCM concentrations, it enhances the slurry's enthalpy gain and provides more thermal energy to be stored. The coconut oil/Au based slurry's thermal energy storage capacity is enhanced from 4.73 to 8.26 by augmenting the mass concentration as seen in Fig. 12. Improving the concentration, on the contrary, increases the heat losses to atmosphere by inducing the temperature to increase more on the upper surface of the slurry in the storage system. This compels the heat gain improvement to be adversely affected. As illustrated in Fig. 12, the useful heat gain

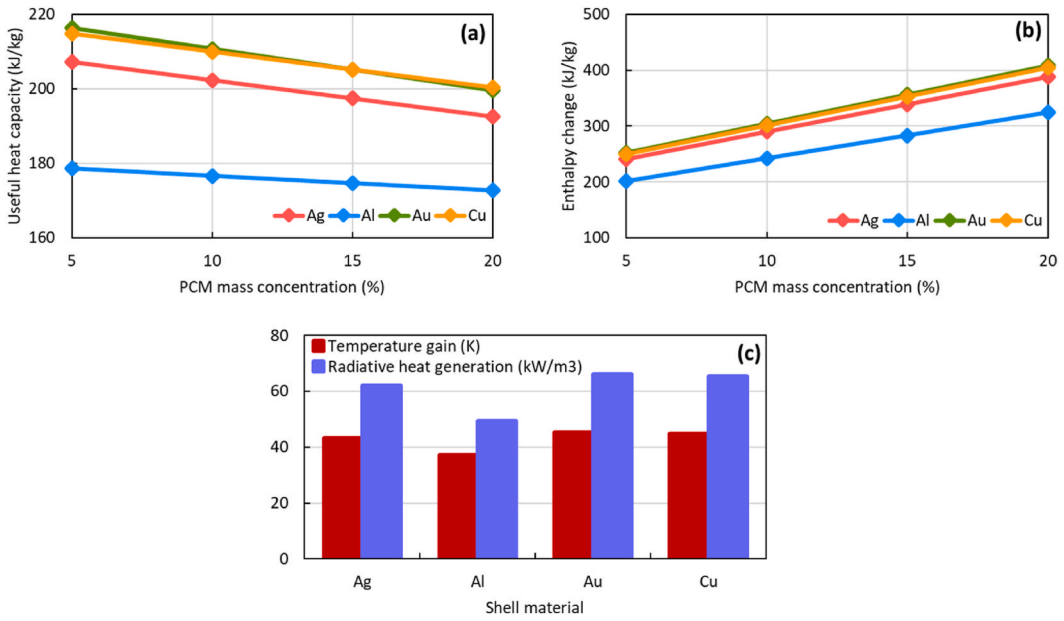

Fig. 13. Comparative analysis of thermal behaviour (a and b) at tilt angle of 30° and (c) at mass concentration of 20 % and tilt angle of 45°.

ability of Au shell-based slurry in diminished from 2.41 to 2.12 as the mass concentration augments. These positive and negative outcomes are consisted with the study of Kazaz et al. [37] who found that as the concentration is enhanced, while the heat loss is negatively affected, the thermal storage is improved.

The change in the tilt angle directly also influences the temperature gain of the storage system. At constant mass concentration and same slurry type, improving the inclination angle from 0 to 60° adversely alters the merged free convection and radiation heat transfer in the cavity. As the inclination angle augments, the buoyancy forces' impact within the collector diminishes and natural convection decreases. Due to this reduced effect, it declines the slurry heat increment by lessening the heat that the nanocapsules can generate by radiation. Enhancing the inclination angle, thus, reduces the sun to thermal energy conversion, resulting in insufficient storage (Fig. 12). This reduction in the thermal performance due to the slope angle accords with the findings of Mamun et al. [69].

The performances of different types of slurries are compared in terms of constant angle in Fig. 13. The PCM mass concentration effect changing at constant tilt angle is demonstrated in Fig. 13(a and b), while the impact of combined constant mass concentration and tilt angle is illustrated in Fig. 13(c). Enhancing the mass concentration augments the nanocapsules' thermal energy conversion capacity, improving the slurry's enthalpy gain and augmenting the thermal energy it can absorb (Fig. 13(b)). However, since this transformation causes too much heat gain on the cavity's upper wall, it increases the heat losses to the surroundings, and diminishes the slurry's useful heat performance (Fig. 13 (a)). Moreover, since Al particles have low optical characteristics and thermal conductivity, the thermal characteristics of coconut oil/Al nanoencapsulated slurry are at the lowest level as temperature gain of 37.17 K and heat generation of 49.35 kW/m^3 (Fig. 13(c)).

4.3.3. Effect of combined inclination angle and core size on thermal performance

The essential factor altering the solar energy to thermal energy conversion is the characteristics of the fluid. The fluid's optical and thermophysical properties contribute to augmenting these capabilities. In the previous section, the coconut oil/Al nanoencapsulated slurry has the lowest capacity. One of the points affecting this performance is the core size. Since the core size not only impacts the optical characteristics but also the thermophysical properties, it is a matter of phenomenon

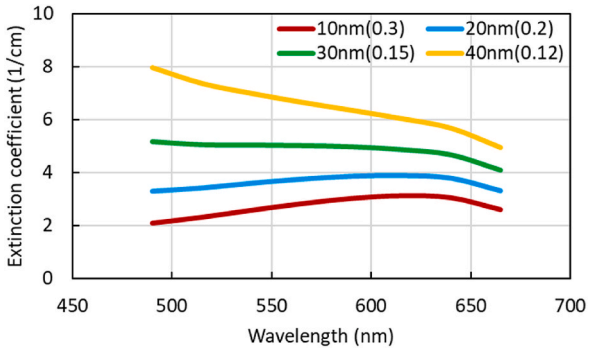

Fig. 14. Impact of *SA/V* on optical properties a function of wavelength.

what effect it will have on the thermal performance.

The variation of core dimension on the extinction coefficient is given as a function of wavelength in Fig. 14. The coconut oil's diameter (*SA/V*, m^{-1}) is defined as 10 (0.3), 20 (0.2), 30 (0.15) and 40 nm (0.12). An increase in the total size means a decline in the *SA/V*. When the core size is 10 and 20 nm, the extinction coefficient increases up to 640 nm with enhancing wavelength, while it decreases along the wavelength at 30 and 40 nm. The probable reason for this is that the Al particles with metallic properties become active in the shell due to the solar radiation and provoke a small peak at 640 nm in wavelength. It is noticed that this peak observation is also obtained in the examination of Wu et al. [34]. It is also recognized that the average attenuation augments with the enhancement of the particle dimension. This finding further supports the viewpoint of Wu et al. [34].

The fluid's optical properties are not a factor impacting the photothermal conversion alone, but its thermophysical properties should also be considered. These two combined effects, thus, allow an understanding of the thermal performance. Fig. 15 exhibits the core size's behaviour on the photothermal conversion characteristics with varying inclination angle. It is obtained that the thermal performance decreases slowly with the improved core size at the fixed tilt angle. Enhancing the coconut oil diameter increases the particle diameter, leading to an improvement in the particle's volume. This volume increase, which provokes a decrease in the *SA/V*, causes agglomeration of the uniformly dispersed nanocapsules in the fluid. This situation deteriorates the heat

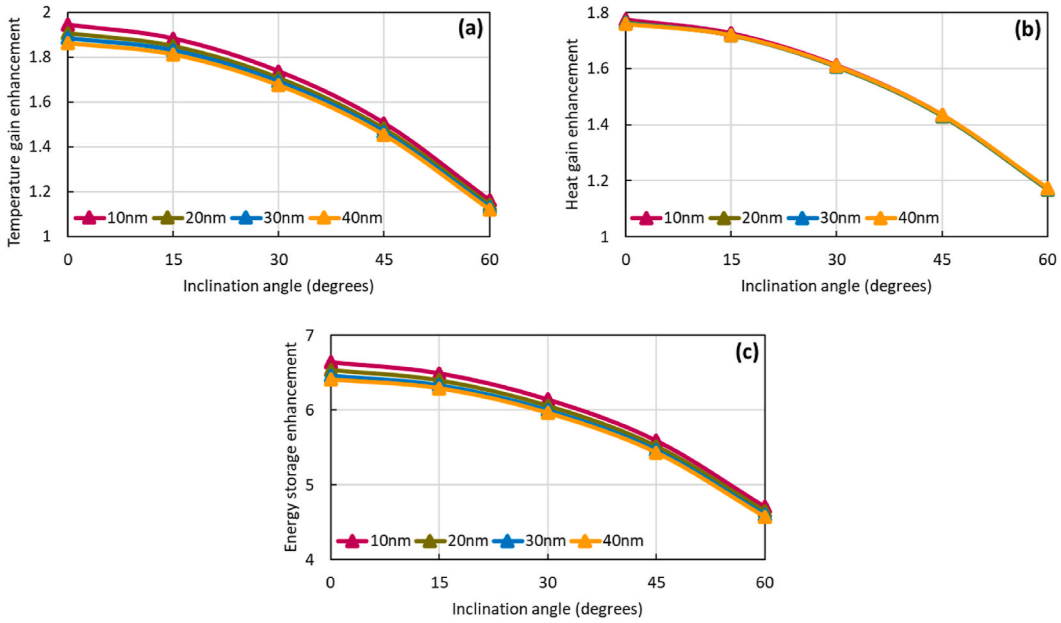

Fig. 15. Impact of core size with varying inclination angle on (a) temperature, (b) heat, and (c) energy storage enhancements.

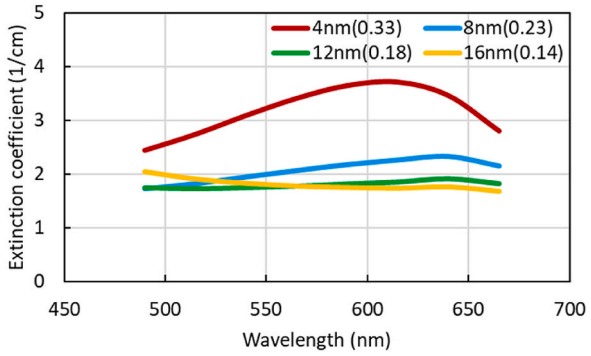

Fig. 16. Impact of *SA/V* on optical properties a function of wavelength.

transfer between nanocapsules and water, preventing the enhancement in the slurry's temperature augmentation (Fig. 15(a)). Due to the decreasing temperature gain, it also alters the slurry's heat increment relatively negatively (Fig. 15(b)). Besides, since the slurry's temperature gain influences the enthalpy change negatively, the thermal energy storage also diminishes slowly with augmenting diameter (Fig. 15(c)). This thermal reduction is consisted with data obtained in earlier inspection of Ashraf et al. [70] who reported that as the particle dimension is augmented, the agglomeration deteriorates the system capacity.

At fixed nanocapsule size, furthermore, reducing the inclination angle augments the solar energy's absorption capacity by the slurry, improving the capacity of the coconut oil/Al nanoencapsulated slurry due to the enhanced light-matter interaction. As the tilt angle decreases, it improves the slurry's buoyancy effect, and also improves the storage system's free convection heat transfer. With the enhancing free

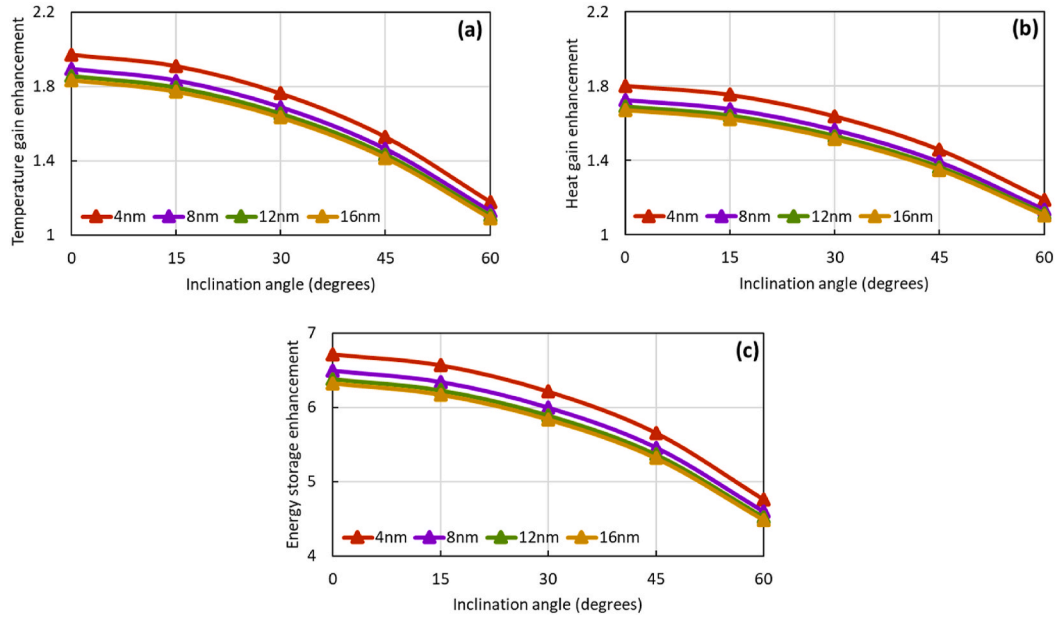

Fig. 17. Impact of shell thickness with varying inclination angle on (a) temperature, (b) heat, and (c) energy storage enhancements.

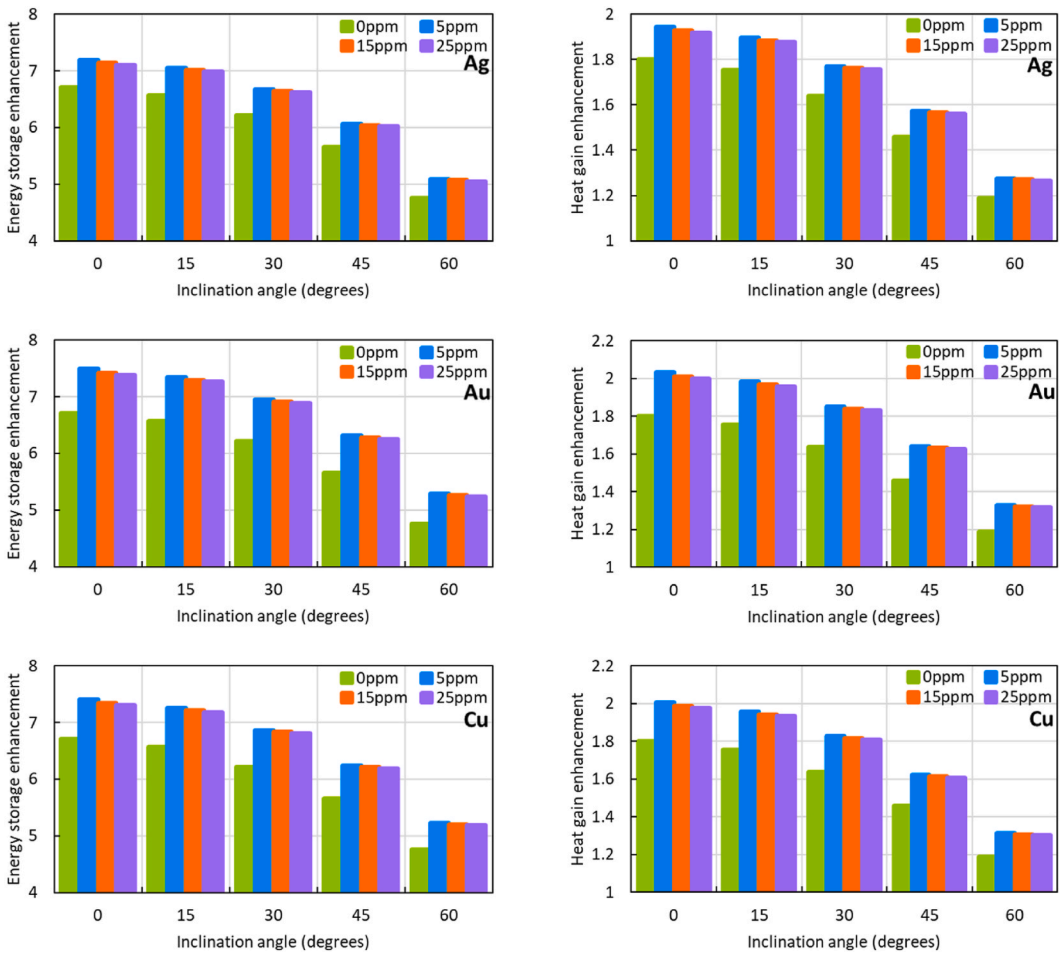

Fig. 18. Impact of mono nanoparticle addition with varying inclination angle on energy storage (left pillar) and heat gain (right pillar) augmentations.

convection, it induces the nanocapsules dispersed in the water to collide with each other more easily, thus augmenting the capacity of capturing sunlight. Thus, the heat generation due to the irradiation in the slurry increases, and the average performance of the slurry improves. For example, when the core diameter is 20 nm, the improvements in temperature, heat gain, and energy storage of the slurry are found to be improved from 1.14 to 1.91 (Fig. 15(a)), 1.17 to 1.76 (Fig. 15(b)), 4.64 to 6.54 (Fig. 15(c)) respectively, with the inclination angle decreasing from 60 to 0°. This thermal enhancement seems to be consistent with the other research conducted by Hachicha et al. [71].

4.3.4. *Effect of combined inclination angle and shell thickness on thermal performance*

Shell thickness is one of the aspects manipulating the nanocapsule's optical properties. Fig. 16 indicates the behaviour of varying shell thickness to the mean extinction coefficient as a function of wavelength. Shell thicknesses (SA/V, m^{-1}) are determined as 4 (0.33), 8 (0.23), 12 (0.18) and 16 nm (0.14). Changing the shell thickness alters the nanocapsule's SA/V. Due to the free electrons of the metallic nanoparticles, it is observed that the peak formation occurs differently in different shell thicknesses. It is unearthed that as the shell width augments, the SA/V of the nanocapsule diminishes, and the peak formation slowly shifts to the larger wavelength. As the SA/V augments, it shifts to the short wavelength, with the peak occurring more clearly. This similarity in shifting is supported by the findings of Lv et al. [33] and Oldenburg et al. [72].

The combined capability of thermophysical and optical properties determines the slurry's photothermal conversion. Fig. 17 is analysed as a function of the changing inclination of the slurry consisting of nanocapsules with different shell thicknesses. Improving the shell thickness at a constant slope angle decreases the slurry's thermal power. Enhancing the particles dimension with shell thickness increases the nanocapsules' volume at constant fraction. This induces a shrinkage in the SA/V of the capsules in the slurry. Nanocapsules, so, cause agglomeration, resulting in insufficient sunlight absorption. Meagre heat generation in slurry, consequently, adversely alters the thermal energy storage system's power. This negativity corroborates the perspective of Kazaz et al. [37] who unveiled that the smaller particle dimension enhances the thermal performance much more.

Moreover, it is marked that the system overall capacity diminishes as the inclination angle of the cavity where the solar energy is stored increases. As the angle enhances, the effect of the lifting force declines, thus limiting the movements of the slurry in the cavity. Nanoencapsulated PCMs dispersed in water, therefore, become more stable, resulting in a reduction in radiation-induced heat generation. For example, when the shell thickness is 8 nm, the temperature, heat, and thermal energy storage gain enhancements of the system decrease from 1.9 to 1.12 (Fig. 17(a)), 1.72 to 1.13 (Fig. 17(b)), and 6.49 to 4.59 (Fig. 17(c)), respectively as the slope augments from 0 to 60°. This diminish reflects those of Shaik et al. [73] who discovered that the thermal reduction increases by enhancing the tilt angle.

4.3.5. *Effect of combined inclination angle and nanoparticle addition on thermal performance*

Heat transfer fluid can be considered as the most substantial element affecting the sun to thermal energy conversion as an energy storage material. Optical and thermophysical properties can be regarded as factors impacting the fluid's capacity. Another technique to improve the performance of coconut oil/Al nanoencapsulated slurry is to form a

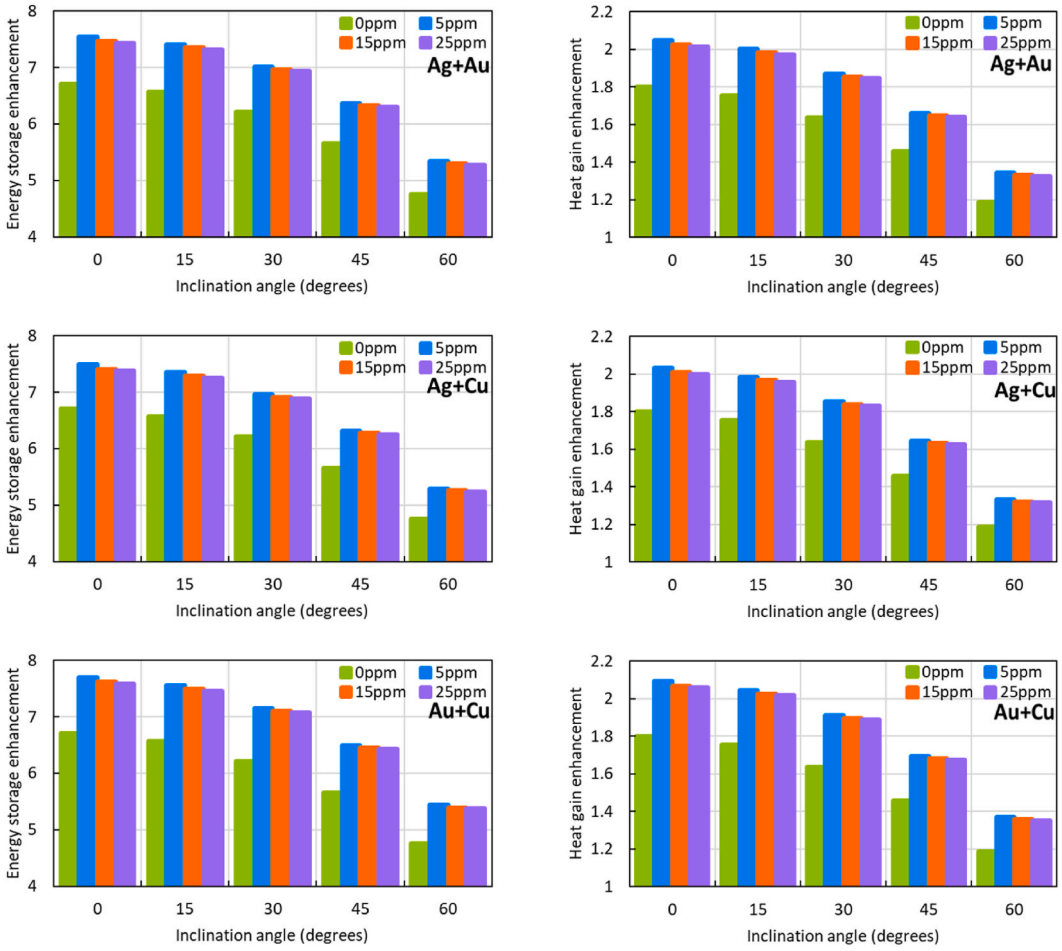

Fig. 19. Impact of hybrid nanoparticle concentration addition with varying inclination angle on energy storage (left pillar) and heat gain (right pillar) augmentations.

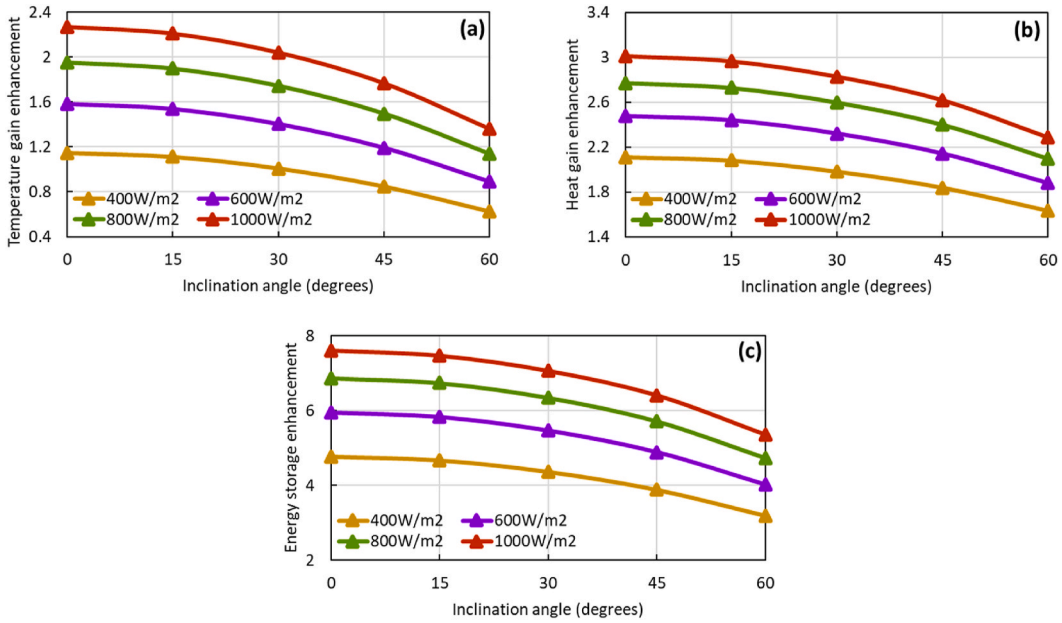

Fig. 20. Impact of heat flux with varying inclination angle on (a) temperature, (b) heat, and (c) energy storage enhancements.

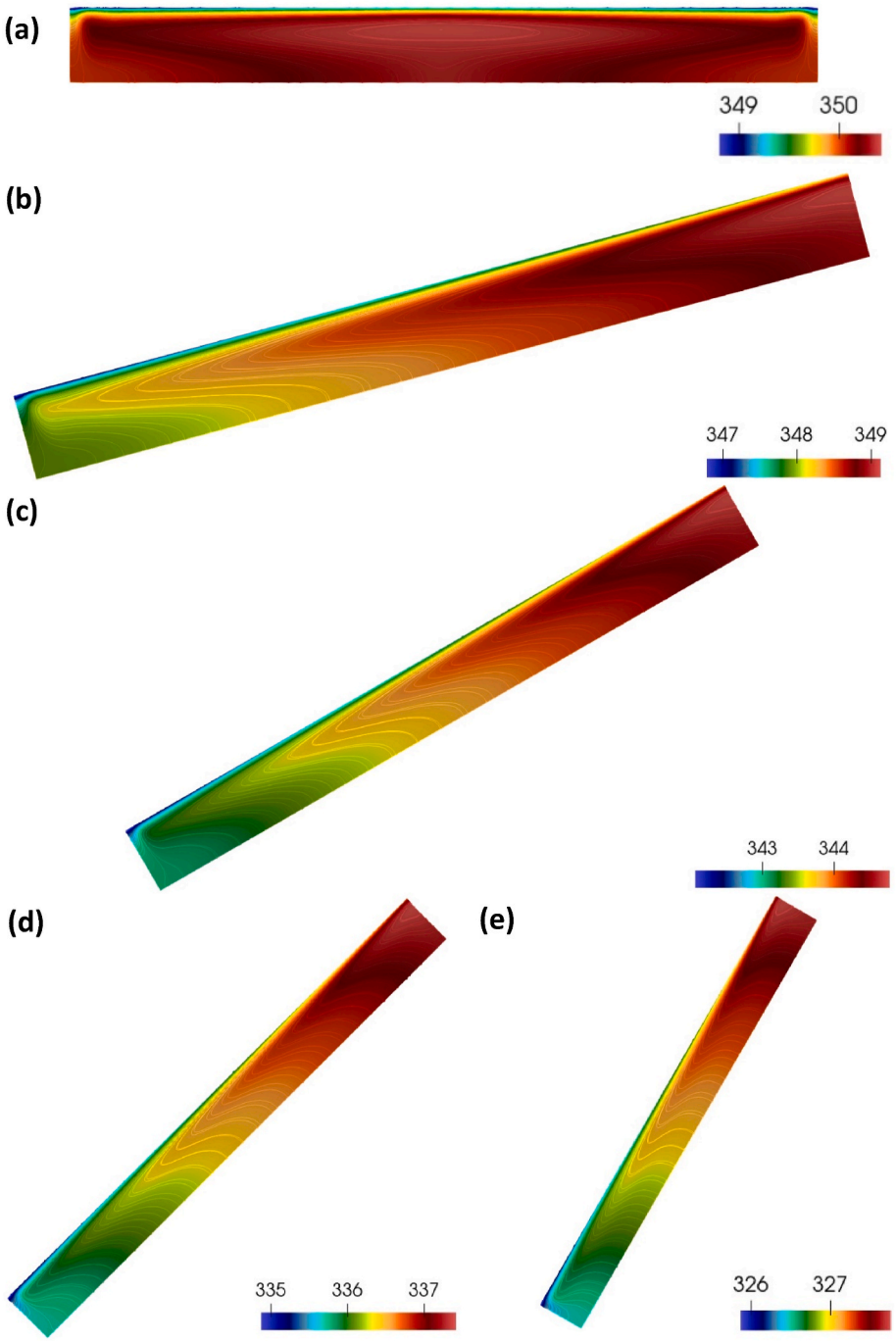

Fig. 21. Temperature (K) contours of coconut oil/Ag slurry at mass concentration of 0.2 for diverse collector slopes: (a) 0, (b) 15, (c) 30, (d) 45 and (e) 60°.

hybrid slurry by adding nanoparticles to the water. The newly formed slurry's optical characteristics reflect the properties of each of the nanoparticle, nanocapsule, and host fluid.

Ag, Au, and Cu nanoparticles are dispersed in coconut oil/Al nano-encapsulated slurry as indicated in Fig. 18. It is seen that the slurry has the lowest capacity when the volume concentration is zero (no nano-particle effect). As the particle concentration augments, it helps the hybrid slurry not only to improve its optical properties, but also to enhance its thermophysical properties. Thanks to this augmentation, it enhances both the fluid's thermal energy storage and heat gain by increasing the ability of the new type of slurry to absorb solar energy.

The application of hybrid nanoparticles is another way to further improve the fluid's capacity. It will improve the slurry's temperature increment by allowing the slurry to catch more sunlight. In Fig. 18, Ag, Au and Cu mono nanoparticles are added, while in Fig. 19 blended particles, which are combinations of these nanoparticles with each other, are formed and dispersed in water. As seen in Fig. 19, the performances of Ag + Au, Ag + Cu and Au + Cu based hybrid slurries are found to be better than Ag, Au and Cu based hybrid slurries. For example, the energy storage improvements of Cu and Ag based slurries enhance by 4.04 and 4.87 %, respectively, with the insertion of Au nanoparticles at a volume fraction of 25 ppm and an inclination angle of 15°. Further, the inclusion of Cu nanoparticles augments the recovery of the Ag based slurry by 4.02 %. The thermal enhancement by mono- and blended-nanoparticles is confirmed by Kazaz et al. [37].

It is expressed that improving the nanoparticle concentration

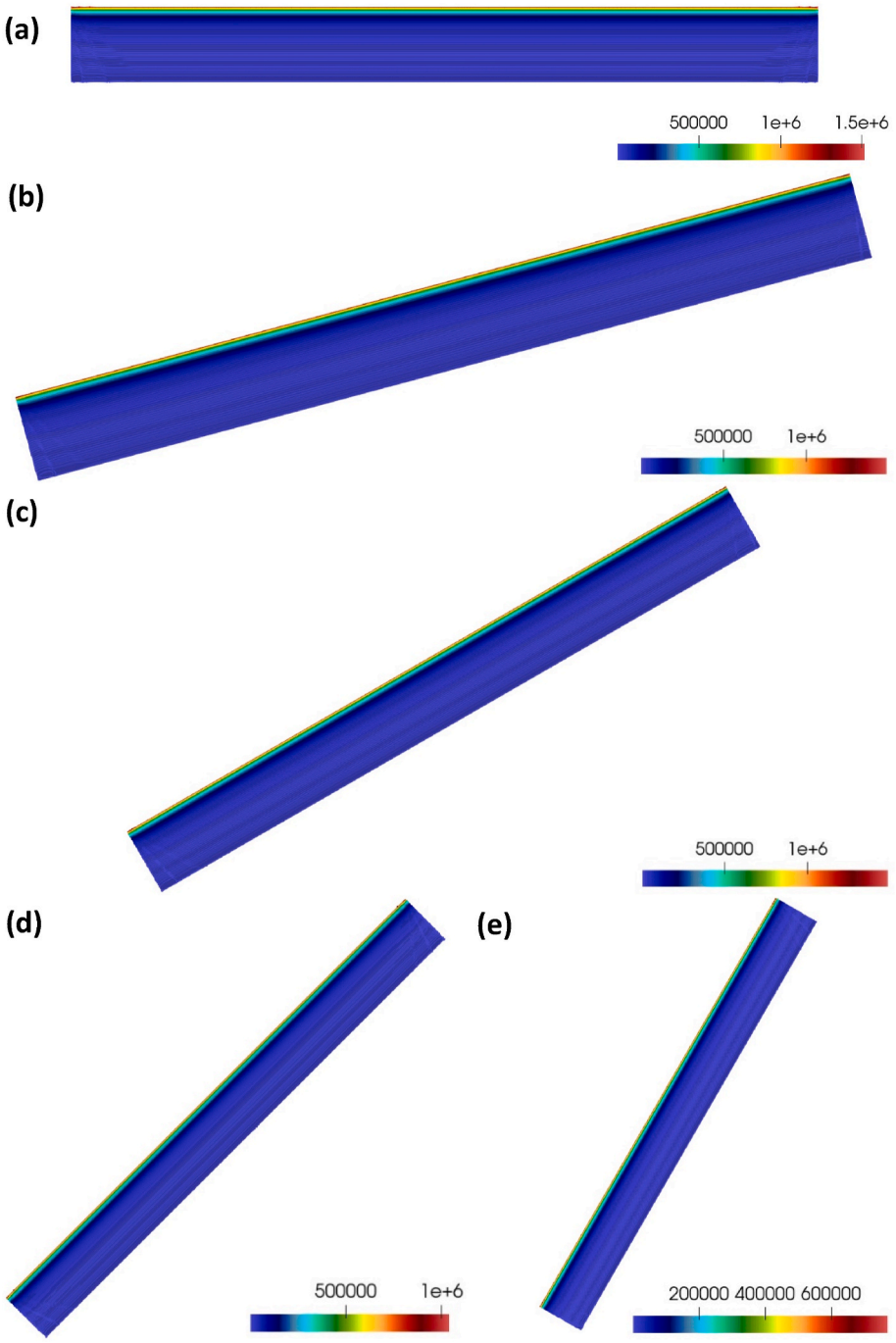

Fig. 22. Volumetric heat generation (Wm^{-3}) contours of coconut oil/Ag slurry at mass concentration of 0.2 for diverse collector slopes: (a) 0, (b) 15, (c) 30, (d) 45 and (e) 60°.

deteriorates the system's capacity in both Figs. 18 and *19*. The concentration increment incites the slurry in the cavity to absorb the radiation less, reducing the heat generation from the radiation. This is because as the concentration enhances, the sun's rays are absorbed more by the hybrid slurry around the cavity's upper panel, causing an increment in the top plate temperature. This augments the heat dissipation from cavity to surrounding and diminishes the system capacity. The former examination of Kazaz et al. [44] revealed the similar outcomes.

Finally, improvement in tilt angle is another point that negatively influences the photothermal conversion. As explained in the previous sections, the merged impacts of thermal radiation and natural convection decrease as the inclination angle improves. Due to the impact of the weak buoyant force, the collision of the molecules and particles forming the slurry is insufficient, causing a lessening in the heat production in the cavity. The overall conversion performance, thus, is reduced.

4.3.6. Effect of combined inclination angle and solar heat flux on thermal performance

Solar radiation intensity is one of the natural factors altering the slurry's thermal. Solar radiation occurs at the maximum level at noon and its effect continues increasing and decreasing from sunrise to sunset. Therefore, it may cause a significant alteration in the temperature gain of the slurry.

The different radiation's impact values solar-to-thermal energy conversion of the slurry is analysed in Fig. 20. Hybrid slurry based on Au + Cu blended particles is considered as fluid due to the higher capacity

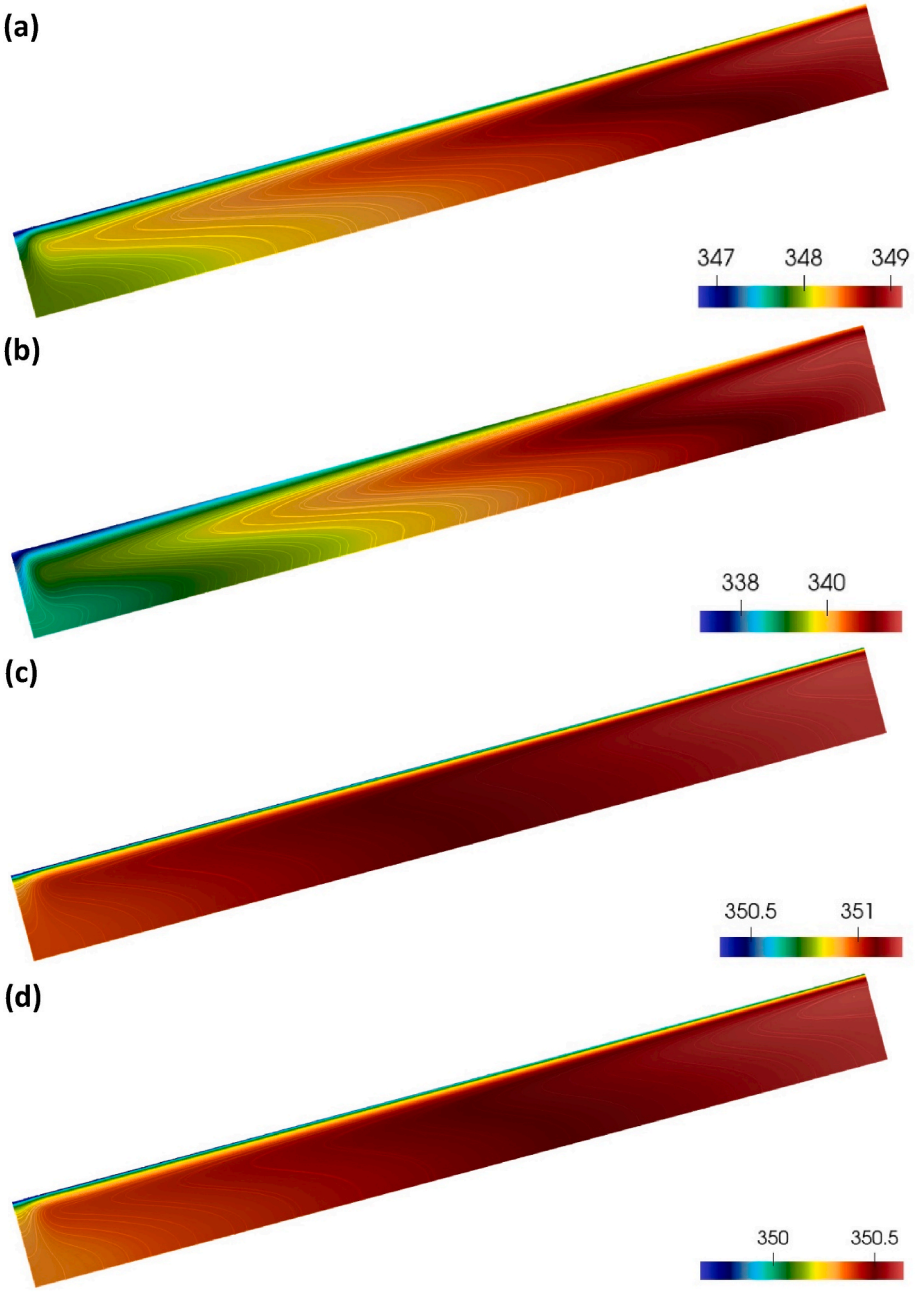

Fig. 23. Temperature (K) contours at inclination angle of 15° and mass concentration of 0.15: coconut oil-based (a) Ag, (b) Al, (c) Au, and (d) Cu slurries.

in the previous section. 400, 600, 800 and 1000 W/m^2 are also determined as solar radiation intensity. Improving the solar heat flux increases the radiation's force penetrating the energy storage material and augments the capacity of the shell structures made of metallic materials to capture this sunbeam. In parallel with the increase in the energy of nanocapsules in the slurry due to sunlight, it enhances the fluid's temperature of the fluid (Fig. 20(a)). This improves the slurry's useful heat capacity (Fig. 20(b)). It, thus, augments the slurry's enthalpy gain, enhancing its energy storage (Fig. 20(c)).

Further, it is remarked that improving the inclination angle of the energy storage system at constant radiation intensity compels a diminish in the performance. The heat transfer in the closed cavity is subject to the buoyancy force due to the increment in the fluid's temperature and radiation. An augmentation in the inclination angle induces a decline in the buoyant force, thus negatively affecting the natural convection behaviours. This obstruction may cause the fluid to move more slowly in the cavity, thus rendering the collision of nanocapsules ineffective. These collisions, which also alter the radiation capture capacity, begin a shrink in heat production by radiation. The storage system's power, hence, is inverse proportion to the tilt angle. For instance, enhancing the slope angle from 0° to 60° at a fixed radiation heat flux of 1000 W/m^2 causes the temperature, useful heat, and enthalpy improvements to diminish from 2.27 to 1.36 (Fig. 20(a)), 3.01 to 2.28 (Fig. 20(b)), and 7.61 to 5.31 (Fig. 20(c)), respectively.

4.3.7. Understanding the flow physics and heat transfer

As an advantage of numerical studies, it is possible to visualize the fluid medium. To understand the fluid physics' effect on heat transfer in depth, the volumetric absorbed radiation and temperature profiles are explained in this section. Visualization of the nanoencapsulated PCM slurry will help prevent this deficiency in the literature.

The impact of varying inclination angle on volumetric absorbed radiation and temperature distributions are exhibited in Fig. 21 and Figure *22*, respectively. Improving the tilt angle (Fig. 21(a–e)) leads to

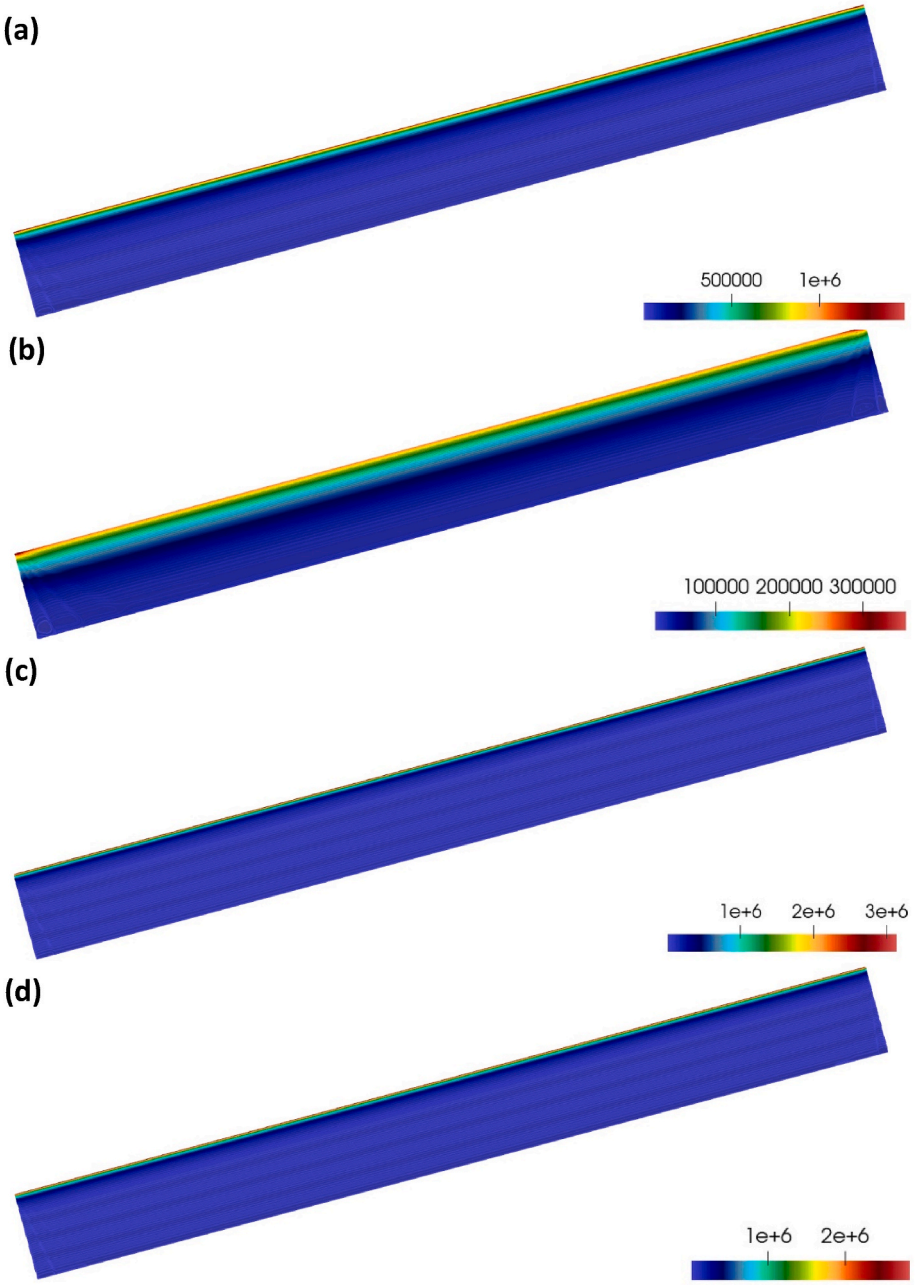

Fig. 24. Volumetric heat generation (Wm^{-3}) contours at inclination angle of 15° and mass concentration of 0.15: coconut oil-based (a) Ag, (b) Al, (c) Au, and (d) Cu slurries.

the nanoencapsulated PCM slurry to not absorb enough radiation due to the reduced penetration of sunlight into the cavity. The slurry's highest temperature, therefore, declines from 350 (Fig. 21(a)) to 327 K (Fig. 21 (e)). This decrease in the temperature reduces the slurry's heat gain and diminishes its thermal energy storage.

To improve the cavity's storage capacity, the base and side walls, which have high reflective characteristics, reflect the sun rays penetrating the cavity towards the cavity's interior by striking these plates. The slurry, whose temperature increases, starts to move upwards from the midpoint of the cavity due to the lifting force (Fig. 21(a)). However, since the cavity's upper panel is covered with a glass plate, it encounters the cold slurry on the upper plate due to heat losses to the atmosphere. It, thus, moves the slurry from top to bottom. Enhancing the collector angle, on the contrary, occasions thermal boundary layers to expand through the length. With the influence of the buoyant force, hence, hot, and cold areas are formed in the upper and base parts of the cavity, respectively.

An augmentation in the inclination angle induces a reduction in the sunlight intensity impacting the nanocapsules. As seen clearly in Fig. 22, it causes a decrease in the slurry's volumetric absorbed radiation and worsens the thermal energy conversion. Metallic shell materials can increase the light scattering in the slurry due to surface plasmon resonance because of radiation. Light scattering in the path of the cavity's bottom, thus, causes a decrease in light intensity. Therefore, it provides an enhancement in the energy that can be produced by the radiation around the upper panel.

The diverse fluids' influence on temperature dissemination inside cavity with an tilt angle of 15° is unveiled in Fig. 23, whereas the heat production from absorbed radiation is illustrated in Fig. 24. It is indicated in Fig. 12 that the absorption capacity improves with the nanocapsule addition due to the pure water's low solar energy absorption ability. The effects of composite PCMs with different metallic shells with a PCM mass concentration of 15 % are also different. Since the low

optical properties of the Al particles induce the sun rays to be absorbed at a lower level compared to other shell materials, radiation heat generation is insufficient as in Fig. 24(b). In addition, the Al particles' low thermal conductivity provokes the low heat transmission in pure water. The combination of these two characteristics results in the lowest temperature gain of the coconut oil/Al slurry as in Fig. 23(b). As explained in Fig. 11, nanocapsules formed by using Ag, Au, and Cu materials with better optical properties in the shell structure can absorb solar radiation more than coconut oil/Al capsules. It, thus, enhances the heat generation in the slurry (Fig. 24(a–c, d)). Thanks to their high thermal conductivity capacities, the slurry's temperature gain is moderately higher (Fig. 24(a–c, d)).

5. Conclusions

Conversion of sunlight to heat and thermal storage in a semi-transparent based low temperature solar system using NBPCMS was analysed. The combined impacts of natural convection-tilt angle and solar radiation-particle interaction in a NBPCMS was done by using coconut oil as PCM for the first time. ANSYS Fluent was deployed to unravel the 2-D radiation, heat, and flow characteristics. The capsule size, shell material, inclination angle, solar heat flux, PCM mass concentration, nanoparticle and its concentration were considered as the key elements influencing the overall conversion and storage capacity. The coconut oil was also employed as a non-paraffin PCM for environmentally friendly energy storage material. The findings revealed that the NBPCMS augmented the solar system's capacity. The useful heat capacity of slurries with Ag, Au, Al, and Cu shell materials was 3.02, 3.12, 2.7 and 3.14 times better than water, respectively due to the optically functional PCM nanocapsules while the thermal energy storage was 8.85, 9.29, 7.41, and 9.19 times higher. Enhancing the core/shell confinement dimension determining by the shell thickness and core also provoked a shrinking in the *SA/V*, enabling the capsules to build up bigger structures at host fluid. This diminished the slurry's thermal energy storage capacity, reducing the heat generation by radiation.

As the PCM mass fraction augmented from 0.05 to 0.2, the slurry's heat gain enhancement diminished while the storage enhanced due to higher phase transformation. In addition, since different capsules had different optical and thermophysical characteristics due to dissimilar shell materials, their slurries performance on conversion and storage were unlike. For example, the thermal energy storage rate of the slurry-based Cu, al, Ag and Au shelled coconut oil core/shell confinements were 6.4, 5.14, 6.16, and 6.48, respectively when the mass concentration and inclination angle were 10 % and 30°. Besides, nanoparticle addition to base fluid were noticed to enhance the slurry's thermal behaviour. The Au nanoparticle-based hybrid slurry further augmented the storage capacity of Ag and Cu shelled based slurries by 4.87 % and 4.04 %, respectively at a volume fraction of 25 ppm and a tilt angle of 15°. It was confirmed that the augmentation in the solar ray's power, which is a natural factor, from 400 to 1000 W/m^2, improves thermal conversion by enhancing the energy of nanocapsules by absorbing more intense sun rays. Moreover, it was clearly found that improving the solar receiver's slope from 0 to 60° reduces the system's performance. The reason for this was that the increasing inclination angle reduced the buoyancy force, causing the slurry to become more stable, diminishing the collision of the particles and reducing the heat generation from the radiation.

Finally, it was observed in the experiments that the melting behaviour of solid coconut oil was affected by wind speed and solar radiation. It was noticed that improving the heat flux caused the solid storage material to melt earlier and the temperature increment was higher. In addition, augmenting the wind velocity increased the heat losses to the atmosphere and induced the melting to start late, thus reducing the temperature gain. In this study, it is clearly seen that the PCM-based nanocapsules improve the converting sunlight to heat and storage due to the surface plasmon resonance vibration of metallic shells. It has been found that coconut oil has suitable and superior properties in the use of PCM. Thus, it has been observed that bio-based PCM and nanocapsules can be used instead of paraffin-based PCMs and contribute to the improvement of decarbonization. Furthermore, the implications of this new kind of heat transfer fluid which is a combination of bio PCM-based nanocapsules and base fluid remains future concept under flow conditions Herein, the combined impacts of fluid velocity and light-matter interaction need to be investigated as 3D. The experimental investigation of these PCM-based nanaocapsules will also be examined.

CRediT authorship contribution statement

Oguzhan Kazaz: Writing – review & editing, Writing – original draft, Visualization, Validation, Software, Methodology, Investigation, Formal analysis, Conceptualization. **Nader Karimi:** Writing – review & editing, Supervision. **Manosh C. Paul:** Writing – review & editing, Supervision, Project administration, Funding acquisition, Conceptualization, Methodology, Resources.

Declaration of competing interest

The authors declare that they have no known competing financial interests or personal relationships that could have appeared to influence the work reported in this paper.

Data availability

Data will be made available on request.

References

[1] Kazaz O, Ferraro R, Tassieri M, Kumar S, Falcone G, Karimi N, Paul MC. Sensible heat thermal energy storage performance of mono and blended nanofluids in a free convective-radiation inclined system. Case Stud Therm Eng 2023;51:103562.
[2] Liu L, Fan X, Zhang Y, Zhang S, Wang W, Jin X, Tang B. Novel bio-based phase change materials with high enthalpy for thermal energy storage. Appl Energy 2020;268:114979.
[3] Sun M, Liu T, Wang X, Liu T, Li M, Chen G, Jiang D. Roles of thermal energy storage technology for carbon neutrality. Carbon Neutrality 2023;2(12):1–54.
[4] Agarwal A, Molwane OB, Pitso I. Thermal analysis & modelling of phase change material used in low temperature industrial wastewater applications. Mater Today Proc 2021;39(Part 1):596–605.
[5] Kazaz O, Karimi N, Kumar S, Falcone G, Paul MC. Computational analysis of the influence of bio based phase change material slurry on the thermal performance in a volumetrically heated solar system. In: 15th international green energy conference (IGEC-XV), glasgow, UK; 2023.
[6] Khargotra R, Alam T, Thu K, András K, Siddiqui TU, Singh T. Influence of heat enhancement technique on the thermal performance of solar water heater for sustainable built environment. Start-of-the-art review. Sustain Energy Technol Assessments 2023;57:103293.
[7] Xiao Y, Huang P, Wei G, Cui L, Xu C, Du X. State-of-the-art review on performance enhancement of photovoltaic/thermal system integrated with phase change materials. J Energy Storage 2022;56(Part C):106073.
[8] Wang D, Liu H, Liu Y, Xu T, Wang Y, Du H, Wang X, Liu J. Frost and High-temperature resistance performance of a novel dual-phase change material flat plate solar collector. Sol Energy Mater Sol Cell 2019;201:110086.
[9] Li J, Zhang W, Xie L, Li Z, Wu X, Zhao O, Zhong J, Zeng X. A hybrid photovoltaic and water/air based thermal(PVT) solar energy collector with integrated PCM for building application. Renew Energy 2022;199:662–71.
[10] Nekoonam S, Ghasempour R. Modeling and optimization of a thermal energy storage unit with cascaded PCM capsules in connection to a solar collector. Sustain Energy Technol Assessments 2022;52(Part C):102197.
[11] Reyes-Cueva E, Nicolalde JF, Martínez-Gómez J. Characterization of unripe and mature avocado seed oil in different proportions as phase change materials and simulation of their cooling storage. Molecules 2021;26(1):107.
[12] Mehrizi AA, Karimi-Maleh H, Naddafi M, Karimi F. Application of bio-based phase change materials for effective heat management. J Energy Storage 2023;61:106859.
[13] Yuan Y, Zhang N, Tao W, Cao X, He Y. Fatty acids as phase change materials: a review. Renew Sustain Energy Rev 2014;29:482–98.
[14] Kahwaji S, White MA. Edible oils as practical phase change materials for thermal energy storage. Applied sciences 2019;9(8):1627.
[15] Alqahtani T, Mellouli S, Bamasag A, Askri F, Phelan PE. Experimental and numerical assessment of using coconut oil as a phase-change material for unconditioned buildings. Int J Energy Res 2020;44(7):5177–96.

[16] Okogeri O, Stathopoulos VN. What about greener phase change materials? A review on biobased phase change materials for thermal energy storage applications. International Journal of Thermofluids 2021;10:100081.
[17] Prasannaa P, Ramkumar R, Sunilkumar K, Rajasekar R. Experimental study on a binary mixture ratio of fatty acid-based PCM integrated to PV panel for thermal regulation on a hot and cold month. Int J Sustain Energy 2021;40(3):218–34.
[18] Chopra K, Tyagi VV, Pathak AK, Pandey AK, Sari A. Experimental performance evaluation of a novel designed phase change material integrated manifold heat pipe evacuated tube solar collector system. Energy Convers Manag 2019;198:111896.
[19] Xu H, Zhang C, Wang N, Qu Z, Zhang S. Experimental study on the performance of a solar photovoltaic/thermal system combined with phase change material. Sol Energy 2020;198:202–11.
[20] Wang C, Cheng C, Jin T, Dong H. Review on bio-based shape-stable phase change materials for thermal energy storage and utilization. J Renew Sustain Energy 2022;14(5):052701.
[21] Nazari M, Jebrane M, Terziev N. Bio-based phase change materials incorporated in lignocellulose matrix for energy storage in buildings—a review. Energies 2020;13(12):3065.
[22] Sami S, Sadrameli SM, Etesami N. Thermal properties optimization of microencapsulated a renewable and non-toxic phase change material with a polystyrene shell for thermal energy storage systems. Appl Therm Eng 2018;130:1416–24.
[23] Wang C, Liang W, Yang Y, Liu F, Sun H, Zhu Z, Li A. Biomass carbon aerogels based shape-stable phase change composites with high light-to-thermal efficiency for energy storage. Renew Energy 2020;153:182–92.
[24] Ghoghaei MS, Mahmoudian A, Mohammadi O, Shafii MB, Mosleh HJ, Zandieh M, Ahmadi MH. A review on the applications of micro-/nano-encapsulated phase change material slurry in heat transfer and thermal storage systems. J Therm Anal Calorim 2021;145:245–68.
[25] Ran F, Chen Y, Cong R, Fang G. Flow and heat transfer characteristics of microencapsulated phase change slurry in thermal energy systems: a review. Renew Sustain Energy Rev 2020;134:110101.
[26] Kazaz O, Karimi N, Kumar S, Falcone G, Paul MC. Enhanced thermal energy storage capacity of solar systems using nano-encapsulated nano size of n-octadecane phase change material as an inorganic shell. In: 2nd world energy conference and 7th UK energy storage conference, birmingham, UK; 2022.
[27] Karami M, Shahini N, Behabadi MAA. Numerical investigation of double-walled direct absorption evacuated tube solar collector using microencapsulated PCM and nanofluid. J Mol Liq 2023;377:121560.
[28] Bohdal T, Dutkowski K, Kruzel M. Experimental studies of the effect of microencapsulated PCM slurry on the efficiency of a liquid solar collector. Materials 2022;15(13):4493.
[29] Yuan K, Wang H, Liu J, Fang X, Zhang Z. Novel slurry containing graphene oxide-grafted microencapsulated phase change material with enhanced thermo-physical properties and photo-thermal performance. Sol Energy Mater Sol Cell 2015;143:29–37.
[30] Raj P, Subudhi S. A review of studies using nanofluids in flat-plate and direct absorption solar collectors. Renew Sustain Energy Rev 2018;84:54–74.
[31] ANSYS fluent user's guide. Canonsburg: ANSYS, Inc.; 2013.
[32] Bohren CF, Huffman DR. Absorption and scattering of light by small particles. New York: Wiley; 1983.
[33] Lv W, Phelan PE, Swaminathan R, Otanicar TP, Taylor RA. Multifunctional core-shell nanoparticle suspensions for efficient absorption. J Sol Energy Eng 2013;135(2):021004.
[34] Wu Y, Zhou L, Du X, Yang Y. Optical and thermal radiative properties of plasmonic nanofluids. Int J Heat Mass Tran 2015;82:545–54.
[35] Duan H, Chen R, Zheng Y, Xu C. Photothermal properties of plasmonic nanoshell-blended nanofluid for direct solar thermal absorption. Opt Express 2018;26(23):29956–67.
[36] Neeves AE, Birnboim MH. Composite structures for the enhancement of nonlinear-optical susceptibility. J Opt Soc Am B 1989;6(4):787–96.
[37] Kazaz O, Karimi N, Kumar S, Falcone G, Paul MC. Heat transfer characteristics of fluids containing paraffin core-metallic shell nanoencapsulated phase change materials for advanced thermal energy conversion and storage applications. J Mol Liq 2023;385:122385.
[38] Kazaz O, Karimi N, Kumar S, Falcone G, Paul MC. Thermally enhanced nanocomposite phase change material slurry for solar-thermal energy storage. J Energy Storage 2024;78:110110.
[39] Hale GM, Querry MR. Optical constants of water in the 200-nm to 200-μm wavelength region. Appl Opt 1973;12(3):555–63.
[40] Palik ED. Handbook of optical constants of solids. Academic Press; 1997.
[41] Yunus WMM, Fen YW, Yee LM. Refractive index and fourier transform infrared spectra of virgin coconut oil and virgin olive oil. Am J Appl Sci 2009;6(2):328–31.
[42] Babar S, Weaver JH. Optical constants of Cu, Ag, and Au revisited. Appl Opt 2015;54(3):477–81.
[43] Duffie JA, Beckman WA. Solar engineering of thermal processes. Hoboken: New Jersey: John Wiley & Sons, Inc.; 2013.
[44] Kazaz O, Karimi N, Kumar S, Falcone G, Paul MC. Enhanced sensible heat storage capacity of nanofluids by improving the photothermal conversion performance with direct radiative absorption of solar energy. J Mol Liq 2023;372:121182.
[45] Kazaz O, Karimi N, Kumar S, Falcone G, Paul MC. Effects of combined radiation and forced convection on a directly capturing solar energy system. Therm Sci Eng Prog 2023;40:101797.
[46] Khanafer K, Vafai K, Lightstone M. Buoyancy-driven heat transfer enhancement in a two-dimensional enclosure utilizing nanofluids. Int J Heat Mass Tran 2003;46(19):3639–53.
[47] Ternik P. Conduction and convection heat transfer characteristics of water–Au nanofluid in a cubic enclosure with differentially heated side walls. Int J Heat Mass Tran 2015;80:368–75.
[48] Sharaf OZ, Al-Khateeb AN, Kyritsis DC, Abu-Nada E. Direct absorption solar collector (DASC) modeling and simulation using a novel Eulerian-Lagrangian hybrid approach: optical, thermal, and hydrodynamic interactions. Appl Energy 2018;231:1132–45.
[49] Sheikholeslami M, Ganji DD, Ashorynejad HR. Investigation of squeezing unsteady nanofluid flow using ADM. Powder Technol 2013;239:259–65.
[50] Saleel CA. A review on the use of coconut oil as an organic phase change material with its melting process, heat transfer, and energy storage characteristics. J Therm Anal Calorim 2022;147:4451–72.
[51] Cengel Y, Boles M. Thermodynamics: an engineering approach. 2015.
[52] Mehling H, Cabeza LF. Heat and cold storage with PCM: an up to date introduction into basics and applications. 2008.
[53] Kumar RR, Samykano M, Pandey AK, Kadirgama K, Tyagi VV. Phase change materials and nano-enhanced phase change materials for thermal energy storage in photovoltaic thermal systems: a futuristic approach and its technical challenges. Renew Sustain Energy Rev 2020;133:110341.
[54] Hosseini M, Ranjbar AA, Sedighi K, Rahimi M. A combined experimental and computational study on the melting behavior of a medium temperature phase change storage material inside shell and tube heat exchanger. Int Commun Heat Mass Tran 2012;39(9):1416–24.
[55] Siyabi IA, Khanna S, Mallick T, Sundaram S. Experimental and numerical study on the effect of multiple phase change materials thermal energy storage system. J Energy Storage 2021;36:102226.
[56] Sodhi GS, Muthukumar P. Compound charging and discharging enhancement in multi-PCM system using non-uniform fin distribution. Renew Energy 2021;171:299–314.
[57] Liu X, Zhang Z, Zhu C, Wang F, Zhao D, Li Z, Liu Y, Zhang H, Jiang H. Experimental investigation on the effect of phase change materials for thermal management improvement of the fast charging power module. Case Stud Therm Eng 2023;42:102711.
[58] Khanna S, Reddy KS, Mallick TK. Performance analysis of tilted photovoltaic system integrated with phase change material under varying operating conditions. Energy 2017;133:887–99.
[59] Kamkari B, Amlashi HJ. Numerical simulation and experimental verification of constrained melting of phase change material in inclined rectangular enclosures. Int Commun Heat Mass Tran 2017;88:211–9.
[60] Tao Y, Liu YK, He Y-L. Effects of PCM arrangement and natural convection on charging and discharging performance of shell-and-tube LHS unit. Int J Heat Mass Tran 2017;115(Part B):99–107.
[61] Fragnito A, Bianco N, Iasiello M, Mauro GM, Mongibello L. Experimental and numerical analysis of a phase change material-based shell-and-tube heat exchanger for cold thermal energy storage. Journal of Energy Storage 2022;56(Part A):105975.
[62] Goel M, Roy SK, Sengupta S. Laminar forced convection heat transfer in microcapsulated phase change material suspensions. Int J Heat Mass Tran 1994;37(4):593–604.
[63] Lee BJ, Park K, Walsh T, Xu L. Radiative heat transfer analysis in plasmonic nanofluids for direct solar thermal absorption. J Sol Energy Eng 2012;134(2):021009.
[64] Nikpourian H, Bahramian AR, Abdollahi M. On the thermal performance of a novel PCM nanocapsule: the effect of core/shell. Renew Energy 2020;151:322–31.
[65] Hu X, Huang Z, Zhang Y. Preparation of CMC-modified melamine resin spherical nano-phase change energy storage materials. Carbohydr Polym 2014;101:83–8.
[66] Qiao G, Lasfargues M, Alexiadis A, Ding Y. Simulation and experimental study of the specific heat capacity of molten salt based nanofluids. Appl Therm Eng 2017;111:1517–22.
[67] Rao Z, Wang S, Peng F. Molecular dynamics simulations of nano-encapsulated and nanoparticle-enhanced thermal energy storage phase change materials. Int J Heat Mass Tran 2013;66:575–84.
[68] Goel M, Roy SK, Sengupta S. Laminar forced convection heat transfer in microcapsulated phase change material suspensions. Int J Heat Mass Tran 1994;37(4):593–604.
[69] Mamun MAA, Islam MM, Hasanuzzaman M, Selvaraj J. Effect of tilt angle on the performance and electrical parameters of a PV module: comparative indoor and outdoor experimental investigation. Energy and Built Environment 2022;3(3):278–90.
[70] Ashraf MA, Peng W, Zare Y, Rhee KY. Effects of size and aggregation/agglomeration of nanoparticles on the interfacial/interphase properties and tensile strength of polymer nanocomposites. Nanoscale Res Lett 2018;13(214):1–7.
[71] Hachicha AA, Al-Sawafta I, Said Z. Impact of dust on the performance of solar photovoltaic (PV) systems under United Arab Emirates weather conditions. Renew Energy 2019;141:287–97.
[72] Oldenburg S, Averitt RD, Westcott SL, J Halas N. Nanoengineering of optical resonances. Chem Phys Lett 1998;288(2–4):243–7.
[73] Shaik S, Vigneshwaran P, Roy A, Kontoleon KJ, Mazzeo D, Cuce E, Saleel CA, Alwetaishi M, Khan SA, Gürel AE, Ağbulut Ü. Experimental analysis on the impacts of soil deposition and bird droppings on the thermal performance of photovoltaic panels. Case Stud Therm Eng 2023;48:103128.